Andean Geology 40 (1): 1-40. January, 2013
doi: 10.5027/andgeoV40n1-a01

Andean Geology
formerly Revista Geológica de Chile
www.andeangeology.cl

Geochemical signatures of tephras from Quaternary Antarctic Peninsula volcanoes

Stefan Kraus[1], Andrei Kurbatov[2], Martin Yates[3]

[1] *Servicio Nacional de Geología y Minería (SERNAGEOMIN), Avenida Santa María 0104, Providencia, Santiago, Chile. stefan.kraus@sernageomin.cl*

[2] *Climate Change Institute, University of Maine, 136 Sawyer, Orono ME 04469, USA. akurbatov@maine.edu*

[3] *Department of Earth Sciences, University of Maine, Bryand Global Sciences Bld., Orono ME 04469, USA. yates@maine.edu*

** Corresponding author: stefan.kraus@sernageomin.cl*

ABSTRACT. In the northern Antarctic Peninsula area, at least 12 Late Pleistocene-Holocene volcanic centers could be potential sources of tephra layers in the region. We present unique geochemical fingerprints for ten of these volcanoes using major, trace, rare earth element, and isotope data from 95 samples of tephra and other eruption products. The volcanoes have predominantly basaltic and basaltic andesitic compositions. The Nb/Y ratio proves useful to distinguish between volcanic centers located on the eastern (Larsen Rift) and those situated on the western side (Bransfield Rift) of the Antarctic Peninsula. In addition, the Sr/Nb ratio (for samples with SiO_2 <63 wt%), along with Sr/Y, Ba/La, Zr/Hf and Th/Nb are suitable to unequivocally characterize material erupted from every studied volcanic center. Microprobe analyses on volcanic glass show that the samples are generally very poor in K_2O, and that glass from Bransfield Rift volcanoes is enriched in SiO_2, while that of Larsen Rift volcanoes tends towards elevated alkali contents. We propose an algorithm for the identification of the source volcano of a given tephra layer using the new geochemical fingerprints. This will contribute to the development of a regional tephrochronological framework needed for future correlations of tephra in climate archives (*e.g.*, marine, lacustrine and ice cores).

Keywords: Late Pleistocene, Holocene, Explosive volcanism, Tephra, Source volcano identification, Geochemical fingerprint, Antarctic Peninsula, Bransfield Rift, Larsen Rift.

RESUMEN. Geoquímica de tefras de volcanes Cuaternarios de la Península Antártica. En la parte norte de la Península Antártica existen, por lo menos, 12 centros volcánicos del Pleistoceno Tardío-Holoceno que podrían representar las fuentes de horizontes de tefra reconocidos en la región. Se reportan aquí análisis químicos de 10 de estos volcanes, que incluyen análisis de elementos mayores, trazas, tierras raras y composición isotópica de 95 muestras de tefra u otros productos eruptivos. Los volcanes tienen, en su mayoría, composición basáltica a basáltico-andesítica. Las razones Nb/Y resultan útiles para distinguir entre centros volcánicos ubicados al lado oriental (Larsen Rift) de aquellos ubicados al lado occidental (Bransfield Rift) de la Península Antártica. Adicionalmente, las razones Sr/Nb (para muestras con SiO_2 <63 wt%), Sr/Y, Ba/La, Zr/Hf y Th/Nb sirven para caracterizar los productos generados por cada centro volcánico. Análisis de microsonda en vidrio muestran que las rocas estudiadas tienen bajos contenidos de K_2O, y que vidrios de rocas provenientes de volcanes ubicados en el rift de Bransfield son ricos en SiO_2, mientras que las de volcanes del rift de Larsen tienden hacía contenidos elevados de álcalis. Se propone un algoritmo para la identificación del volcán de origen de un horizonte de tefra cualquiera, basado en las distintivas composiciones geoquímicas aquí reportadas. Este estudio contribuirá al desarrollo de un marco tefrocronológico regional indispensable para futuras correlaciones de tefra en distintos registros paleoclimáticos (por ejemplo, testigos de sedimentos marinos y lacustres, núcleos de hielo).

Palabras clave: Pleistoceno Tardío, Holoceno, Volcanismo explosivo, Tefra, Volcán de origen, Huella geoquímica, Península Antártica, Rift de Bransfield, Rift de Larsen.

1. Introduction

In the northern part of the Antarctic Peninsula there are at least a dozen volcanic centers that are (or have been in the past) potentially capable of dispersing volcanic ash over large areas (Fig. 1). Over the past few decades, a range of studies on the volcanic products generated by these volcanoes (Baker *et al.*, 1975; Palais and Kyle, 1988; Björck *et al.*, 1991a, 1993; Hodgson *et al.*, 1998; Smellie, 1999a, b, 2001; Fretzdorff and Smellie, 2002; Fretzdorff *et al.*, 2004; Gibson and Zale, 2006; Kraus and Kurbatov, 2010) has contributed to the development of a tephrochronological framework that can be used to identify potential source volcanoes within the Antarctic continent. Unfortunately, published data on the timing of the volcanic activity and geochemistry of the erupted products are only available for a limited number of volcanic centers (LeMasurier and Thomson, 1990; Björck *et al.*,1991a; Wilch *et al.*, 1999; Smellie, 2002; Harpel *et al.*, 2008; Kraus and Kurbatov, 2010; Smellie *et al.*, 2011). Paucity of available samples is related to complicated fieldwork logistics (*e.g.*, Smellie, 1999a), and thus prevents the development of a comprehensive database of chemical analyses from the Antarctic Peninsula region. For example, there are only sparse published chemical compositional data on the glass component

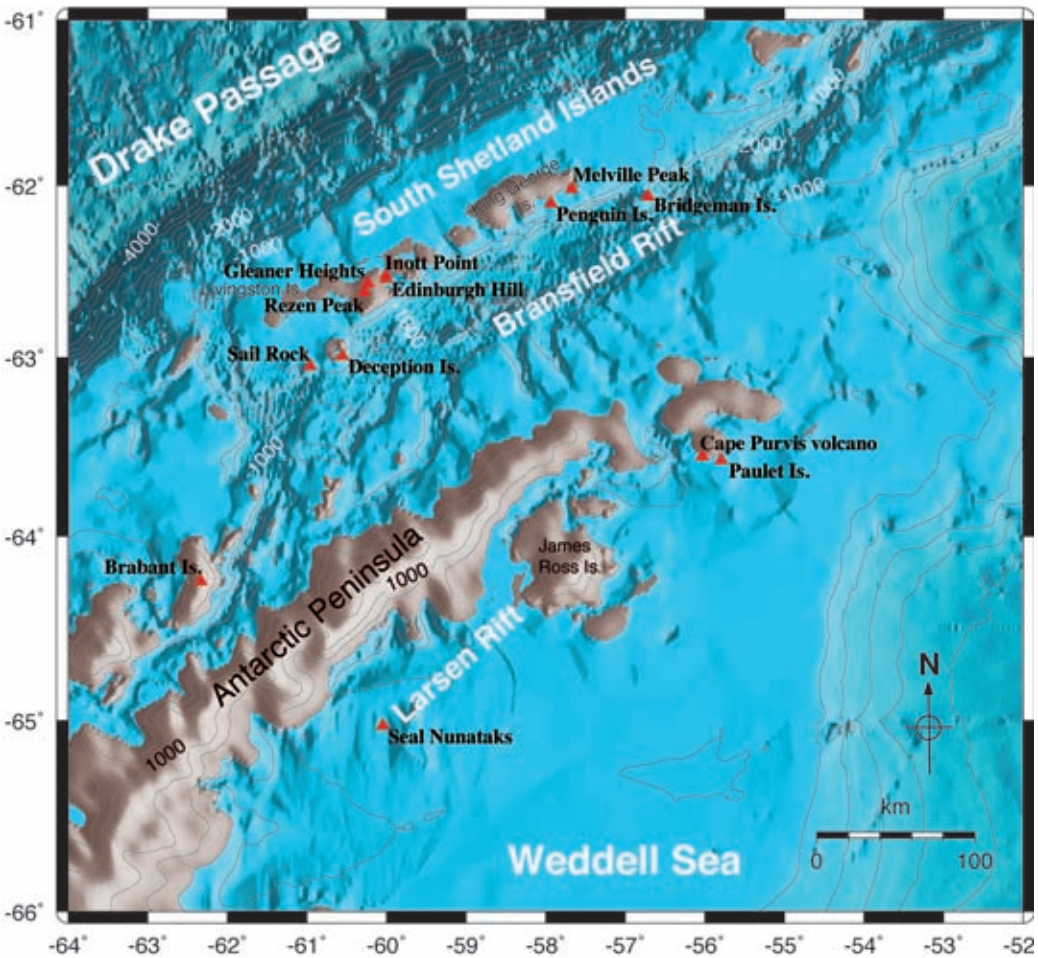

FIG. 1. Map of the northern Antarctic Peninsula region showing the distribution of Late Pleistocene-Holocene volcanic centers that are important potential sources for tephra layers. The complex tectonic evolution of the region led to the formation of Bransfield Rift on the western and Larsen Rift on the eastern side of the peninsula, resulting in unique geochemical fingerprints of the eruption products.

of pyroclastic material for the northern Antarctic Peninsula area (Hodgson *et al.*, 1998; Moreton and Smellie, 1998; Pallás *et al.*, 2001; Fretzdorff and Smellie, 2002), a comprehensive study, however, is missing. Recent studies in other regions (Alloway *et al.*, 2007; Pearce *et al.*, 2007) demonstrate that trace element signatures could provide a unique chemical 'fingerprint' for individual volcanic centers, because trace elements tend to vary more strongly between different volcanoes than major elements do, refining considerably the resulting geochemical information. In particular, trace and rare earth element ratios (*e.g.*, Zr/Hf, Nb/Y or Sr/Y) as well as the isotopic composition (Sr, Nd, Pb) could provide a powerful tool for correlating volcanic products using geochemical fingerprinting, even for rocks in advanced alteration stages (*e.g.*, Kraus, 2005; Kraus *et al.*, 2008, 2010).

Identification of tephra sources in numerous paleoclimate archives (ice cores, lake and marine sediment cores) relies on physico-chemical characteristics of microscopic tephra particles and the timing of the specific volcanic eruption. Tephra particles have been found in every deep Antarctic ice core, *e.g.*, in Byrd (Kyle *et al.*, 1981; Palais and Kyle, 1988), Dome C (Kyle *et al.*, 1981; De Angelis *et al.*, 1985), Dome Fuji (Fujii *et al.*, 1999; Narcisi *et al.*, 2001), Siple Dome B (Dunbar *et al.*, 2003), South Pole (Palais, 1985; Palais *et al.*, 1987; Palais *et al.*, 1989; Palais *et al.*, 1990a; Palais *et al.*, 1992; Cole-Dai *et al.*, 1999), Talos Dome (Narcisi *et al.*, 2001, 2010), Taylor Dome (Dunbar *et al.*, 2003), and Vostok (Palais *et al.*, 1989; Basile *et al.*, 2001). Several tephra layers originating from West Antarctica were recognized in East Antarctica (Basile *et al.*, 2001; Narcisi *et al.*, 2005; 2006). Björck *et al.* (1991a, b, c, 1993) reported a tephrochronological record covering the last 5 ka for the northern part of the Antarctic Peninsula. Fourteen tephra layers were identified visually and by magnetic susceptibility analyses in lake sediments and moss banks.

Despite the recognition of tephra from Antarctic Peninsula volcanoes in paleoclimate records, unresolved potential for Antarctic Peninsula tephrochronology remains. Further development of the tephrochronological framework yields the potential to tie Antarctic paleoclimate archives to other regions, as well as to provide globally linked time stratigraphic markers within different paleoclimate archives. A recent attempt using major elements was made by Hillenbrand *et al.* (2008).

In this work we undertook comprehensive sampling at ten volcanic centers, and subsequent geochemical (microprobe, ICP-MS) and isotopic (Sr, Nd, Pb) analyses.

This article presents a comprehensive geochemical dataset on compositions of tephra and other volcanic products from Late Pleistocene-Holocene Antarctic Peninsula volcanoes, including trace and rare earth element signatures and Sr-Nd-Pb isotopy. We discuss differences for every sampled volcanic center and provide geochemical signatures that can be used for future discrimination of volcanic products in paleoclimate archives.

2. Geological background

Active volcanism in Antarctica is restricted to Marie Byrd Land, parts of the Ross Sea, and the Antarctic Peninsula (LeMasurier and Thomson, 1990; González-Ferrán, 1995). In the latter region, a magmatic arc developed from late Triassic to recent times as part of the Andean-West Antarctic continental margin (*e.g.*, Barker 1982; Barker *et al.*, 1991; Larter and Barker, 1991). During the Cretaceous, the focus of arc magmatism shifted towards the western edge of the Antarctic Peninsula, leading to the development of a separate magmatic arc (Pankhurst and Smellie, 1983; Smellie *et al.*, 1984; Birkenmajer *et al.*, 1986a, b, 1991). That same area became separated from the Antarctic Peninsula by rifting processes acting from Pliocene times onwards, opening the Bransfield Strait (Fig. 1) and thus creating the South Shetland Islands archipelago as a separate crustal block (*e.g.*, Griffiths *et al.*, 1964; Ashcroft, 1972; Davey, 1972; Birkenmajer *et al.*, 1990; Larter and Barker, 1991). The youngest phase of arc magmatism in the Antarctic Peninsula region is therefore preserved in the area of the South Shetland Islands. About 4 Ma ago, the spreading center in the western Drake Passage became inactive (Barker, 1976, 1982; Barker *et al.*, 1991; Larter and Barker, 1991). Subsequently, the South Shetland trench was partly filled with sediments. Today, this last part of the formerly much larger subduction zone is the only area around the entire Antarctic continent where relative movement between the downgoing slab and the overriding plate still takes place, though at very low velocities (Barker, 1982; Robertson Maurice *et al.*, 2002, 2003). The convergence rate should resemble that of the opening of Bransfield Strait, which was estimated at approximately 10 mm/a

(Dietrich *et al.*, 2000). Convergence along the former South Shetland subduction zone is also suggested by seismic data. The earthquake locations indicate that seismicity is associated with slow subduction of young lithosphere, rifting, active volcanism and transcurrent plate boundaries (Robertson Maurice *et al.*, 2002, 2003). Convergence rates between 2.5 and 7.5 mm/a have been estimated for the South Shetland trench for the last 2 Ma (Henriet *et al.*, 1992), based on the amount of stretching and the width of new oceanic crust generated in the Bransfield Strait area, and on the displacement of the South Shetland archipelago to the NW.

However, Bransfield Strait might not be a simple back-arc basin *sensu stricto*, as its opening during the last 4 Ma (*e.g.*, Larter and Barker, 1991) is possibly related to sinistral simple-shear couple between the Scotia and the Antarctic plates (González-Casado *et al.*, 2000), and not to a previously suggested slab rollback mechanism (Barker, 1982). Extensional processes on the eastern side of the Antarctic Peninsula are also responsible for the volcanism along the Larsen Rift (González-Ferrán 1983, 1995), stretching from the Seal Nunataks in the southwest to Cape Purvis and Paulet Island volcanoes in the northeast (Fig. 1).

The modern manifestation of volcanism on both sides of the northern Antarctic Peninsula was shaped during the Late Cenozoic geodynamic evolution. Bransfield Rift on the western, and Larsen Rift on the eastern side of the Antarctic Peninsula were developed in particular during the Late Neogene-Quaternary periods (González-Ferrán, 1983). The modern geotectonic setting and tectonic history are reflected in the geochemistry of the regional volcanic products (our new data show, *e.g.*, characteristically high Nb/Y ratios for the volcanoes located along the intra-plate Larsen Rift).

Recognition of the origin of magmatic material at continental margins is often a difficult venture, due to the possible mixing of subducted sediments and oceanic crust with continental mantle and crust. Reported four different magma sources (Kraus 2005; Machado *et al.*, 2005; Kraus *et al.*, 2008, 2010) contributed to Paleogene arc magmatism in the area of the South Shetland Islands. These sources include subducted sediments, slab derived fluids, the mantle wedge and the continental crust underlying the arc. Because of the longevity of subduction at the Shetland trench (>140 Ma; Pankhurst and Smellie, 1983), a typical subduction zone influence on magma sources is likely, at least for the volcanoes located along the Bransfield Rift.

Subducted sediments as one of the possible contributors to magma formation beneath Bransfield Rift might be reflected by enrichment of the light rare earth elements (LREE) relative to heavy rare earth elements (HREE), generally high Th abundances also expressed as high Th/Ce and low U/Th, moreover low Ta/Nd and Nb/Nd, high Pb isotope ratios, low εNd values and negative Ce anomalies (Hawkesworth *et al.*, 1997; Turner and Hawkesworth, 1997; Turner *et al.*, 2000; Elliott, 2003). Trace element ratios such as Ce/Pb, Zr/Hf, Y/Ho and Nb/Ta, on the other hand, closely reflect the compositions of the magma sources in the upper mantle beneath the rift and are largely unaffected by partial melting and differentiation processes at shallow levels (Hofmann *et al.*, 1986; Miller *et al.*, 1994).

3. Previous work

Existing geochemical literature on the Quaternary volcanism in the Antarctic Peninsula area contributed to establish major regional geochemical characteristics of the volcanism. In an early study by Weaver *et al.* (1979), geochemical features of magmas from Penguin, Deception and Bridgeman islands were explained by fractional crystallization, while inter-volcano variations were attributed to different mantle sources. Keller *et al.* (1992) produced data further supporting the idea that low-pressure fractional crystallization is dominantly responsible for the compositional variation within individual volcanoes. However, interpretation of inter-volcano differences remained difficult.

Baker *et al.* (1975), Smellie (1990), Keller *et al.* (1992) and Smellie *et al.* (2002) reported on the petrology and geochemistry of Deception Island. The geological units sampled by Keller *et al.* (1992) and Smellie *et al.* (2002) comprise pre-caldera as well as post-caldera phases of the island, ranging from basalts to SiO_2-rich trachytes. The high Na_2O, Sr, Zr, and Nb characteristics, but low K_2O, Ba, Rb and Cs are unique signatures of the Deception Island basaltic andesites, differentiating them from nearby seamounts in Bransfield Strait. At comparable MgO concentrations, Deception Island volcanics have higher incompatible element concentrations (except

for the alkalis) than, *e.g.*, Bridgeman Island. For the studied stratigraphic units, Keller *et al.* (1992) stated that there is no correlation between isotope ratios and parameters sensitive to fractional crystallization like SiO_2 and MgO. This implies that either no crustal contamination took place during shallow level magma chamber differentiation, or that it occurred at insignificant levels. However, this conclusion is only valid for the geological units from which Keller *et al.* (1992) took their samples, information that could not be given in the respective paper because it was published before the stratigraphy related information (Baraldo and Rinaldi, 2000; Smellie, 2001) became available.

In the Antarctic Peninsula area, several tephra layers (Björck *et al.*, 1991a, b, c, 1993) were correlated between Livingston Island, Elephant Island, Hope Bay and James Ross Island. Unfortunately, no geochemical data are available from most localities, and the correlations were made using radiocarbon ages. Most of these tephra layers were attributed to Deception Island.

Deception Island has also been suggested as origin of numerous other Holocene tephra layers in ice, lake and marine sediment cores found in the northern Antarctic Peninsula (Smellie, 1999a, and references therein). The latest event (1871 A.D.) evident in Antarctic continent ice cores that was attributed to Deception Island was reported from the Siple Dome ice core (Kurbatov *et al.*, 2006). A tephra layer dated 1816-1821 A.D. was found in a South Pole ice core (Palais *et al.*, 1989), likely also originating from Deception Island, as well as the 1641 A.D. and 1636 A.D. events reported from another South Pole ice core (Delmas *et al.*, 1992; Budner and Cole-Dai 2003, respectively). The latter two might reflect the same eruption that was determined as 1641±3 A.D. in a James Ross Island ice core (Aristarain *et al.*, 1990; Aristarain and Delmas, 1998), 1639 A.D. at Plateau Remote (Cole-Dai *et al.*, 2000), 1643 A.D. at Talos Dome, East Antarctica (Stenni *et al.*, 2002) and 1641 A.D. on Amundsenisen by Traufetter *et al.* (2004). All these data are based on geochemistry of ice tephras, suggesting that Deception Island is a potential source of tephra layers in different parts of the Antarctic continent and that several times during the past 500 years its tephra has been distributed over large distances.

Penguin Island (Fig. 1) has been suggested as source of a 1.6 m thick, 5.2-3.8 ka tephra layer identified (Tatur *et al.*, 1991) in lake sediments at Fildes and Potter peninsulas (both King George Island). Matthies *et al.* (1988) mention an ash layer from marine sediments cored in Bransfield Strait, part of which could have originated from Bridgeman Island. No age or chemical analyses are published from this tephra.

Fretzdorff and Smellie (2002) investigated the volcanic history at Deception, Bridgeman and Penguin islands. Like other authors, they attributed most ash layers found in gravity cores from Bransfield Strait to Deception Island, corroborating that volcano as the most likely source of tephra layers in the region.

However, the study also identified an ash layer of unknown origin, but based on the shallow stratigraphical position in which the layer was found, the authors concluded that the source volcano must have been active in historical times and its compositional characteristics suggested it had a Bransfield Strait source. Keller *et al.* (2002) and Fretzdorff *et al.* (2004) present comprehensive geochemical and isotopic datasets on the submarine volcanism and along-axis chemical variations of the Bransfield Rift.

While extensive literature exists on Bransfield Rift and the associated Quaternary volcanism, literature on Larsen Rift is much sparser. The term 'Larsen Rift' was established by González-Ferrán (1983), referring to an actively extending structure in the area.

A short description of the mainly Pliocene to Quaternary James Ross Island Volcanic Group (JRIVG) associated with Larsen Rift is given by Lawver *et al.* (1995), along with some chemical analyses of the eruption products. Hole (1990) and Hole *et al.* (1993) report on the chemical and isotopic composition of Pliocene to recent intraplate basalts from the Seal Nunataks (Fig. 1) and draw conclusions on their mantle source and eventual heterogeneities of the asthenosphere beneath the Antarctic Peninsula.

The volcanic and climatic history of James Ross Island are described by Smellie *et al.* (2006a), and detailed descriptions of the volcanic lithofacies of the James Ross Island Volcanic Group are given in Smellie *et al.* (2008). The volcanism described by these authors lasted at least six million years and produced both an extensive volcanic field and one of the largest stratovolcanoes in Antarctica.

Chemical and isotope compositions of alkaline lavas from northern James Ross Island were presented by Košler *et al.* (2009), along with a discussion on the

petrogenesis, the character of their magma sources and differences in chemical composition between arc and back-arc settings.

Four tuff and cinder cones located on the eastern side of James Ross Island are perfectly preserved and suggest a potential Holocene age. Three of them (Eugenia volcano, Marina volcano, and Elba volcano) were described by Strelin *et al.* (1992). Eventual Holocene activity on James Ross Island is consistent with the results of high-resolution airborne gravity imaging which indicates the presence of a low-density sub-surface body beneath parts of James Ross Island that could be interpreted as a partially molten magma chamber (Jordan *et al.*, 2007).

Eruptive processes, age and geology of the Cape Purvis volcano (together with Paulet Island the northernmost representative of the James Ross Island Volcanic Group) are outlined in Smellie *et al.* (2006b).

4. Results from fieldwork and description of the investigated volcanoes

During austral summers 2006/07, 2007/08, 2008/09 and 2009/10, S. Kraus carried out the fieldwork around the northern Antarctic Peninsula. Because of logistic problems and difficult weather conditions, fieldwork at some localities (*e.g.*, Sail Rock, Figs. 1, 2) was reduced to a very short stay. The islands Deception, Penguin, Bridgeman and Paulet count among the volcanic centers where fieldwork could successfully be completed, as well as Melville Peak on King George Island, the Cape Purvis volcano on Dundee Island and Rezen Peak, Inott Point and Edinburgh Hill on Livingston Island (Fig. 1).

Fieldwork on Deception Island was carried out in December 2006. All stratigraphic units identified by Smellie (2001) were sampled. Fieldwork at the other localities was undertaken during austral summers 2007/08, 2008/09 and 2009/10. Some of the locations originally scheduled for fieldwork (Gleaner Heights, James Ross Island, Brabant Island) remained inaccessible due to meteorological and logistic difficulties, but could be partly compensated by additional fieldwork at Inott Point and Edinburgh Hill (Fig. 1). Fieldwork at the Seal Nunataks was impossible for the same reasons, but E. Domack (Hamilton College, New York) in February 2010 kindly collected and provided a sample from Larsen Nunatak, which was included in this study. For volcanic centers sparsely covered by our own samples (Sail Rock, Seal Nunataks), additional analytical data were taken from literature (Hole, 1990; Keller *et al.*, 1992; Hole *et al.*, 1993).

Fieldwork focused strongly on tephra at the respective localities. In case there was more than one stratigraphical unit, we attempted to obtain tephra samples from each unit. In case no tephra could be found, sampling focused on the freshest material available from other glass-rich eruption products (chilled margins, pumice, etc.). Depending on the outcrop situation, 5-10 samples of about 2 kg each were taken at every volcanic center.

4.1. Sail Rock

Very limited information is available on Sail Rock, a small volcano located some 35 km southwest of Deception Island. It rises about 30 m above sea level and features a sail-like shape (hence its name). The stack marks the top of a volcano the rest of which is submerged below sea level. The age of Sail Rock is unknown, and the stack is composed of layers of pyroclastic breccia and tuffs alternating with lava flows (Fig. 2). It was not discovered before March 1987 (Fretzdorff and Smellie, 2002). The only previously published chemical analysis (WR, Keller *et al.*, 1992) was obtained from a plagioclase-phyric, reddish andesite sample similar to some of the Deception Island dacites. This sample was taken in the eighties at the foot of the stack during the only previous visit to this island (E. Godoy, personal communication, 2008; Keller *et al.*, 1992).

Our visit to Sail Rock is the second ever reported. On January 26th, 2008, we collected by helicopter a sample of reddish basaltic andesite from about 1.5 m below the top. No sampling of the pyroclastic units was possible due to the difficult outcrop conditions (Fig. 2). The sampled rock shows macroscopically almost no alteration and a high percentage of clear feldspar phenocrysts.

4.2. Deception Island

Deception Island, the largest and most active volcano in the area, is situated ~40 km south of Livingston Island close to the nascent spreading axis of the immature Bransfield basin (Fig. 1). The upper crustal structure of the area comprises continental crust north of Deception Island and more basic crust to the south (Muñoz-Martín *et al.*, 2005). The tectonic setting of the volcano has been reported as

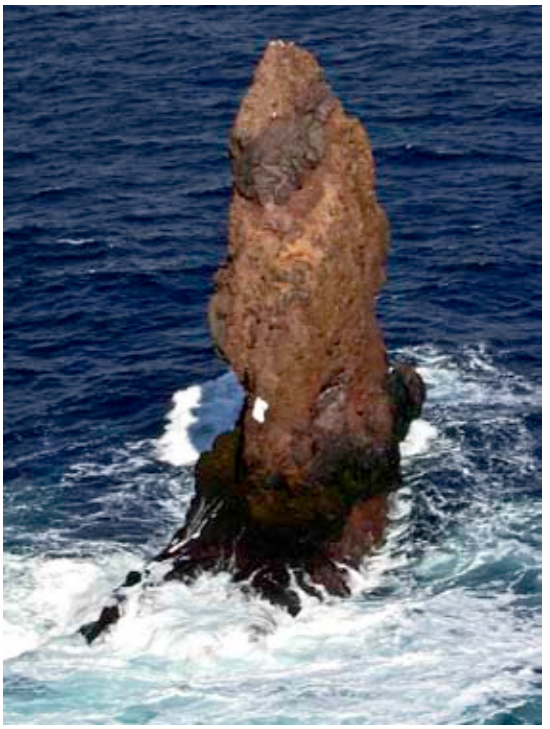

FIG. 2. Sail Rock is the remaining uppermost part of a submerged volcanic edifice, rising ~30 m above sea level. Our sample was taken from a section consisting of interbedded layers of pyroclastic deposits (lighter, reddish parts) and blocks of lava ~1.5 m below the top, underlain by a lava flow (dark brown layer dipping to the left).

extensional, with the maximum horizontal shortening in NE-SW and NW-SE directions (Pérez-López *et al.,* 2007) and local compressional stress states (Maestro *et al.*, 2007).

Smellie (1990) describes Deception Island as a large basalt-andesite shield volcano with a submerged basal diameter of ~30 km and an elevation of *ca.* 1.500 m above the sea floor of its highest summit (Mount Pond, 540 m). The initial emergence of the volcano above sea level likely began with low energetic tephra eruptions from multiple centers (Smellie, 2001). Subsequently, a small basaltic shield was formed by subaerial effusive to weakly pyroclastic activity. The formation of the 10 km wide caldera (Port Foster) marks a turning point in the complicated history of pre- and post-caldera eruptions, but the timing of this important event is unknown. Whether the caldera formed during a continuous extension process (Rey *et al.,* 1995; Martí *et al.,* 1996) or a single catastrophic event (Smellie, 2001) is still under debate. Terminating the pre-caldera phase, Smellie (2001) argues in favor of a catastrophic caldera forming event producing a minimum of ~30 km^3, possibly as much as 60 km^3 (Ben-Zvi *et al.,* 2007, 2009) of magma involving substantial amounts of water, likely seawater. He suggests that the eruption resulted in caldera collapse, followed by several smaller, incremental collapse events, for which there is seismic refraction evidence (Smellie *et al.,* 2002). This particular eruption marks an important change in the eruptive behavior of the volcano, also likely reflecting a change in the magmatic system as a whole. Smellie (2001) notes that petrologic analyses of the juvenile component suggest two distinct magma types in the outer coast tuff possibly related to an important magma mingling event, based on analysis of volatiles (Smellie *et al.*, 1992) and trace elements (Smellie *et al.*, 2002).

According to Smellie (2001), eruptions during the post-caldera phase were characterized by small volumes and were predominantly of phreatomagmatic type.

The recent volcanic activity in Port Foster (the flooded caldera of Deception Island) has been studied by Baker *et al.* (1975), Smellie (2002), Smellie *et al.* (2002) and Somoza *et al.* (2004). Two intense seismic crises in 1992 and 1999 have been interpreted as related to uplift episodes due to deep injections of magma which did not reach the surface, thus indicating the high potential for future volcanic eruptions (Ibáñez *et al.,* 2003).

At least three eruptions have taken place in the last century. The first two of them have been observed directly as they happened during austral summer (1967, 1969). A research party was sent to Deception Island shortly after the end of the third eruption (1970). For this 1967-1970 eruptive cycle, there were published reasonably detailed descriptions of the precursory phenomena, the eruptions themselves, eruption-induced events and the deposits (Shultz, 1972; Baker *et al.,* 1975; Smellie, 2002), but no in-depth geochemical study of the eruption products.

The present activity is expressed by strong hydrothermal circulation and intense seismicity with frequent volcano-tectonic and long-period events (Zandomeneghi *et al.,* 2009). Low P-wave velocities beneath the caldera floor have been interpreted as indication of an extensive magma chamber beneath a sediment-filled basin, extending downwards from $\leq$2 km depth (Ben-Zvi *et al.,* 2007, 2009; Zandomeneghi *et al.,* 2007, 2009). Recent seismic

activity comprises pure seismo-volcanic signals such as volcanic tremor and long-period (LP) events, and volcano-tectonic (VT) earthquakes. The frequency of the LP events varies between 30/day and *ca.* 100/h, the rate of VT events is even more unbalanced (Ibáñez *et al.*, 2003).

In December 2006, we sampled tephra layers and other volcanic products originating from the different eruptive episodes of the volcano (according to the stratigraphy set up by Smellie 2001) as comprehensively as possible at *in situ* outcrops. A total of 37 samples was taken.

4.3. Rezen Peak, Inott Point and Edinburgh Hill (Livingston Island)

The youngest series of volcanic rocks on Livingston Island is represented by the Plio-Pleistocene to Recent (<1 Ma) Inott-Point-Formation (Smellie *et al.*, 1995, 1996). It consists of fresh, vesicle-rich lavas, bombs, tuffs and lapilli-tuffs, which were erupted from multiple small monogenetic centers, including those at Gleaner Heights, Inott Point and Edinburgh Hill volcanoes and are located in central and eastern Livingston Island (Fig. 1). These volcanic edifices are partly subaerial, partly subglacial. In the latter case, eruption products frequently consist of palagonitized tuff. The description of two outcrops along with geochemical data from Rezen Peak was published by Veit (2002). We were not successful in accessing the Gleaner Heights outcrop, but visited and sampled Rezen Peak, Inott Point and Edinburgh Hill.

While Rezen Peak (Fig. 3) shows all the characteristics of a tuya-like subglacial volcanic center (no tephra or other pyroclastic material, flat top with pillow lavas), Inott Point is partly composed of thick pyroclastic units (lapilli tuffs) indicating subaerial activity (Fig. 4).

Edinburgh Hill is a Quaternary volcanic neck located south of Inott Point at the northeastern shore of Livingston Island (Fig. 1). The strongly columnar jointed dolerite plug measures about 250 m in diameter and is about 100 m high (Fig. 5). The volcanic edifice that originally must have been towering above the neck has been completely eroded away, most possibly due to glacial activity. This implies that the age of Edinburgh Hill is probably (Late) Pleistocene. A similar argument might be raised for Inott Point, which is also strongly degraded, but its preservation of less resistant lapilli tuffs as well as a plug suggests that it might be younger and thus a potential source for tephra.

FIG. 3. View of Rezen Peak, central Livingston Island, showing its flat-topped, tuya-like morphology that suggests it is an extinct subglacial volcanic center.

Edinburgh Hill is situated close to a postulated NE striking Cenozoic strike-slip fault (Smellie *et al.*, 1995). Reactivation of this structure during the Pliocene-Pleistocene opening of Bransfield Strait might be the reason for the young volcanism (Smellie *et al.*, 1996). Because of its probably pre-Holocene age, which renders Edinburgh Hill an unlikely source of tephra layers found in the Antarctic Peninsula area, it was not included in our geochemical study.

4.4. Penguin Island

This island volcano is situated close to the southeastern shore of King George Island, thus being located at the northwestern margin of the Bransfield Rift, which separates the South Shetland Islands from the Antarctic Peninsula crustal block. Penguin Island measures between 1.4 and 1.8 km in diameter and covers an area of 1.84 km^2. It has been assigned a Pleistocene-Holocene age (Barton, 1965; González-Ferrán and Katsui, 1970; Birkenmajer, 1980, 2001) and has been related to the recent (<4 Ma) opening of Bransfield Strait.

A prominent, exceptionally thick (up to 1.6 m) ash layer found in two lakes on King George Island (Potter and Fildes peninsulas) has been attributed to this small volcanic island (Tatur *et al.*, 1991), but no chemical data were provided to support this assumption. The absence of glaciers on Penguin Island is no evidence of heat flow and thus a young age because the island is too small to form glaciers,

FIG. 4. Inott Point as seen from Edinburgh Hill, northeastern Livingston Island. It consists of two major outcrops: a well-preserved, partly columnar jointed volcanic neck (left side) and a ~100 m thick sequence of pyroclastic rocks (right side), the latter indicating subaerial activity of this volcanic center.

FIG. 5. Edinburgh Hill in eastern Livingston Island. The strongly columnar jointed dolerite plug measures about 250 m in diameter and approximately 100 m in height and is located at the south shore of Inott Point.

but the volcano's cones and craters are very well preserved, which indeed strongly indicates activity during Holocene times.

4.5. Melville Peak (King George Island)

Melville Peak is a Quaternary, partly eroded subaerial volcanic edifice located in northeastern King George Island (Fig. 6). Traditionally, it was assigned a Pleistocene age and it is assumed to have been inactive during the Holocene (Birkenmajer and Keller, 1990).

An ash layer found by Keller *et al.* (2003) in a marine sediment core in northeastern Bransfield Strait is distinctly different in composition from the Deception Island ashes, but similar to published analyses from Melville Peak volcano (Keller *et al.*, 1992), located about 30 km northwest of the core location. This ash layer is the first known hint of Holocene eruptive activity at Melville Peak volcano. There are no radiocarbon dates from the core, but the authors assume this eventual Melville Peak eruption may have occurred only several thousand years ago (Keller *et al.*, 2003).

FIG. 6. View of Melville Peak volcano, located in northeastern King George Island. Traditionally assigned a Pleistocene age based on isotopic dating, an ash layer recently found in a marine sediment core (Keller *et al.*, 2003) suggests possible Holocene activity.

4.6. Bridgeman Island

Bridgeman Island measures 900 by 600 m and reaches a maximum height of 240 m. It is a remnant of a now inactive Late Pleistocene-Holocene stratovolcano situated on a small submarine platform (Birkenmajer, 1994). There is some conflicting evidence (active fumaroles were reported on Bridgeman Island between 1821 and 1850) that the volcano might have been active during the 19th century (González-Ferrán and Katsui, 1970) but recent landings suggest that it is an inactive volcanic remnant (Birkenmajer, 1994) of an originally much larger volcanic edifice, eroded and now largely submerged beneath the sea, similar to Sail Rock. A marine ash layer identified in a Bransfield Strait sediment core was attributed to this volcano by Matthies *et al.* (1988). Large parts of the steeply inclined summit area are composed of unconsolidated, intensely red tephra.

4.7. Cape Purvis volcano (Dundee Island)

The Cape Purvis volcano is a promontory about 550 m high located in the southern part of Dundee Island (southeastern Antarctic Sound, Fig. 1). It is one of the youngest and northernmost satellite centers of the James Ross Island Volcanic Group (Smellie *et al.*, 2006a, b). The same authors state that part of this volcano's history was characterized by relatively voluminous activity (at least 6 km^3 of lava and breccia; not recalculated to dense rock equivalent). Chemical analyses and age determinations were obtained from a subaerial lava flow cropping out at about 240 m a.s.l. on the southwestern slope of the volcano. It forms part of one of the younger units and is a fresh alkaline basaltic (hawaiite) rock (Smellie *et al.*, 2006b). The $^{40}Ar/^{39}Ar$ age of this lava was determined as 132±19 ka. However, the top of the Cape Purvis volcano, suspected by the same authors to represent the tuff cone core of the volcanic edifice and responsible for the youngest phase of activity, at least, had never been visited. The Cape Purvis volcano probably erupted at the end of the glacial period corresponding to Isotope Stage 6 and the outcrop characteristics suggest that the ice sheet at that time had a minimum surface elevation 300-400 m higher than at present (Smellie *et al.*, 2006b).

On February 4th, 2008, we investigated and sampled the outcrops located on the northern slopes of the Cape Purvis volcano (Fig. 7). The sampling site is located at about 360 m a.s.l. and is composed primarily of pyroclastic rocks resembling pyroclastic density current (ground surge) deposits. Only a short 10-minute investigation and sampling of the outcrops at the top of the volcano was possible (Fig. 8). The outcrops at the summit of the Cape Purvis volcano comprise *ca.* 1,000 m^2; they are entirely surrounded by the ice cap covering the slopes of the volcano. The outcrops consist of pyroclastic rocks (lapilli tuffs) incorporating clasts of basaltic lava up to 30 cm across. Time was too short for a detailed study of the depositional environment, but the thin stratification observed in many parts and the occurrence of basaltic

clasts could indicate a vent-proximal ground surge type origin for the deposits, similar to the outcrops found lower down on the northern slopes. The reddish color of some parts of the outcrops indicates a nearby vent as heat source.

FIG. 7. Possible ground surge deposits on the northern slope of Cape Purvis Volcano at 370 m a.s.l.

FIG. 8. The top of Cape Purvis Volcano (553 m a.s.l.). The pyroclastic rocks represent most possibly vent-proximal ground surge deposits and contain dm-sized clasts of basaltic lava.

4.8. Paulet Island

Located *ca.* 10 km east of Cape Purvis volcano, Paulet Island represents a small volcanic island featuring three craters and one maar. A basal, flat-lying older lava series yielded an imprecise K-Ar age of 300±100 Ka (Baker *et al.*, 1977). The overlying pyroclastic cones have not been dated so far but their age was estimated at only a few thousand years, suggesting at least two periods of eruptive activity (Smellie *et al.*, 2006b). The slopes of the cinder cone are covered by red and black scoria and tephra. On its western slope, a lateral fissure produced basaltic lava flows. The age relationship between the main summit and this lateral fissure remains unknown at present but both are probably of Holocene age, because their excellent state of preservation indicates post-glacial formation and the possibility of Holocene activity (Fig. 9).

We sampled lava from the vicinity of the historic Nordenskjöld hut close to the northern beach. No tephra deposits were recognized there. Tephra, scoria and lava samples were collected from the younger part of the volcanic edifice, including the summit crater and the before mentioned lateral fissure.

4.9. Seal Nunataks

The Seal Nunataks are a Pliocene to recent volcanic field piercing the Larsen ice shelf on the eastern side of the Antartic Peninsula (Fig. 10). The island group is made up of 16 individual nunataks that are composed of basaltic and basaltic andesitic tephra, subaerial lava flows, subglacial pillow basalts and associated hyaloclastites (González-Ferrán, 1995; Smellie and Hole, 1997). The largest of them features a summit elevation of 368 m and covers not more than about 4 km^2 (Hole, 1990; Hole *et al.*, 1993). The volume of eruptive products is relatively small. Some outcrop descriptions and geochemical data were also provided by Veit (2002). In 1982, fumarolic activity at two of the nunataks was reported by González-Ferrán (1995) but remains unconfirmed and observations in 1985 revealed no evidence for recent activity (J.L. Smellie, personal communication, 2012). Activity was also reported from at least two other nunataks about 90 years earlier in 1893 (Larsen, 1894), although there is no evidence for that activity preserved today.

FIG. 9. View of Paulet Island, a small volcanic edifice located close to the southeastern exit of the Antarctic Sound. It has a basal platform primarily composed of basaltic lava flows of Late Pleistocene age, and a largely unmodified, probably Holocene cinder cone with a well-formed summit crater on top of it.

FIG. 10. View of part of the Seal Nunataks, a Quaternary group of volcanoes piercing the Larsen ice shelf on the eastern side of the Antarctic Peninsula. Basalt fragments observed all over a small part of the outer northern edge of the Larsen C ice shelf in early 2010 indicate possible recent activity in the vicinity (E. Domack, personal communication, 2010). Photo courtesy E. Domack.

During a recent helicopter flight over the outer northern edge of the Larsen C ice shelf, coarse basalt debris were observed spreading all over a small part of the ice shelf, possibly originating from some recent eruption in the vicinity (E. Domack, personal communication, 2010). A similar observation was made by M.J. Hole in 1985 but attributed to aeolian tephra redistribution (J.L. Smellie, personal communication, 2012).

Our fieldwork at Seal Nunataks proved impossible due to meteorological and logistic problems, but E. Domack kindly provided one lava sample from Larsen Nunatak, which is included in the work presented here.

5. Methodology and sample stock

The full analytical dataset can be downloaded from the IEDA website (http://dx.doi.org/10.1594/IEDA/100052), gives additional information on sample rejection/analysis rejection (in case of microprobe analyses), recalculation methods (major elements volatile free, Fe_2O_3 recalculated as FeO_t), and quotes the literature data we used to compensate failed fieldwork at Seal Nunataks and poor sample number at Sail Rock.

Except for Deception Island, the grade of alteration is in all cases very low to zero. Only on Deception Island, part of the older pyroclastic units exhibits

substantial grades of palagonitization, shedding some doubt on the reliability particularly of the major element data from these locations.

A total of 95 samples was collected at 10 different volcanic centers. Of these, 55 are tephras, 6 are other glass containing material (chilled margins, pumice and obsidian), and 34 are lavas, bombs, scoria and clasts. Additionally, 17 ice tephras were recovered from different glaciers in central Livingston Island in order to check whether the new dataset would actually allow identifying unequivocally their source volcano (cf. Pallás *et al.*, 2001).

In the first step, thin sections from each sample were examined to determine state of alteration, glass content and grain size. Glass from samples not showing advanced alteration was analyzed at the University of Maine using a Cameca SX-100 electron microprobe using wavelength dispersive spectroscopy (WDS). All analyses were performed using a 15kV, 10nA, 5µm beam, simple silicate and oxide standards and 20 second counts. Sodium and silica were analyzed first to minimize beam damage drift. Matrix corrections were performed applying the X-Phi method of Merlet (1994). Samples were rejected in case they yielded too few analyses or turned out to be inhomogeneous, individual analyses were rejected in case of water contents >3 wt%, dubious glass, totals too high, and low or suspect sodium.

Following standard petrographical work, the samples were prepared at Universidad de Chile (Santiago) for geochemical analyses using an agate mortar. ICP-MS and Sr-Nd-Pb isotope WR analyses were carried out at Activation Laboratories (Ontario, Canada). Bulk geochemical compositions of 81 samples were determined on a wide range of major, trace and rare earth elements (10 major and 45 trace and rare earth elements), applying the ICP-MS technique.

A total of 21 Sr-Nd-Pb isotope analyses was carried out on samples from localities where such data were unavailable from literature. In contrast to the major element composition, the isotopic composition of volcanic glass should be identical to the bulk-rock isotopic composition from the same eruption. Rb and Sr were separated using conventional cation-exchange techniques. The analysis was performed on a Triton multi-collector mass-spectrometer in static mode. During the period of work the weighted average of 15 SRM-987 Sr-standard runs yielded 0.710258±9 (2σ) for $^{87}Sr/^{86}Sr$. Sm and Nd were separated by extraction chromatography on HDEHP covered teflon powder. The analysis was performed on a Triton multi-collector mass-spectrometer in static mode. $^{143}Nd/^{144}Nd$ ratios are relative to the value of 0.511860 for the La Jolla standard. Pb was separated using the ion-exchange technique with Bio-Rad 1x8. Pb isotope compositions were analyzed on a Finnigan MAT-261 multicollector mass spectrometer. The measured Pb isotope ratios were corrected for mass fractionation calculated from replicate measurements of Pb isotope composition in NBS SRM-982 standards. External reproducibility of lead isotope ratios ($^{206}Pb/^{204}Pb$=0.1%, $^{207}Pb/^{204}Pb$= 0.1%, $^{208}Pb/^{204}Pb$=0.2%) on the 2σ level has been demonstrated through multiple analyses of standard BCR-1.

Additionally, the bulk compositions of the 17 ice tephras from central Livingston Island were determined, also using the ICP-MS technique. No isotope analyses were carried out on them. We normalized both the microprobe and the ICP-MS major element data to 100% volatile free in order to make them comparable. The resulting geochemical dataset was processed using the program R (http://www.r-project.org).

Incipient rifting and back-arc settings allow for a large variety of possible processes in the evolution of magmatic systems and their contamination by recycled crust. To characterize each of the Late Pleistocene-Holocene volcanic centers precisely and to separate them reliably from each other, we applied a combination of Rare Earth Elements (REE), High Field Strength Elements (HFSE) systematics and isotope data (Sr, Nd, Pb). Large Ion Lithophile Elements (LILE) are widely used to trace alteration processes that depend on climatic conditions and therefore might differ considerably, while HFSE provide a useful tool to distinguish between different eruptive cycles. Sr, Nd and Pb isotope systems allow characterizing magma sources, detecting eventual crustal contamination and determining the geotectonic setting.

6. Geochemical characteristics of the northern Antarctic Peninsula's Quaternary volcanoes

6.1. ICP-MS major element compositions

Most samples are basalts and basaltic andesites, along with the respective trachytic variations. The majority of the volcanic centers form well-defined

clusters in the TAS diagram (Fig. 11), indicating a narrow compositional range of the respective volcanoes. Only samples from Deception Island, Bridgeman Island and the Seal Nunataks spread over a wider range.

In case of Deception Island, our new data show a slightly different pattern as compared with previously published datasets concerning the total alkali content, particularly when comparing with the data published by Smellie *et al.* (2002). Most of these authors' samples plot tightly around the basaltic andesite - basaltic trachyandesite limit in the TAS diagram, mostly above the subalkali/alkali series boundary. In contrast, our data show a much larger variability concerning the total alkali content at comparable SiO_2-values, both towards higher as well as lower total alkali contents (Fig. 11). Because neither our sample preparation procedures nor the analytical results from (internationally approved) standards measured along with our samples suggest any laboratory-related or analytical problems, we suspect that inter-laboratory differences or the sample sites chosen during fieldwork might be responsible for the observed differences.

While Paulet Island is entirely of trachybasaltic composition, Rezen Peak, Inott Point and Penguin Island have only basaltic chemistry. Using Mg# as differentiation index, Melville Peak shows by far the most primitive composition, whereas Paulet Island, Inott Point and some samples from Cape Purvis and the Seal Nunataks feature the lowest SiO_2 contents (Fig. 12). The very high magnesium numbers shown by the Melville Peak samples indicate rapid ascend of magma, short storage times in a shallow level magma chamber and little or no interaction with continental crust.

The only pronounced evolved whole rock compositions were observed as one dacitic sample from Bridgeman Island and two trachydacitic samples from Deception Island (Figs. 11, 12). The

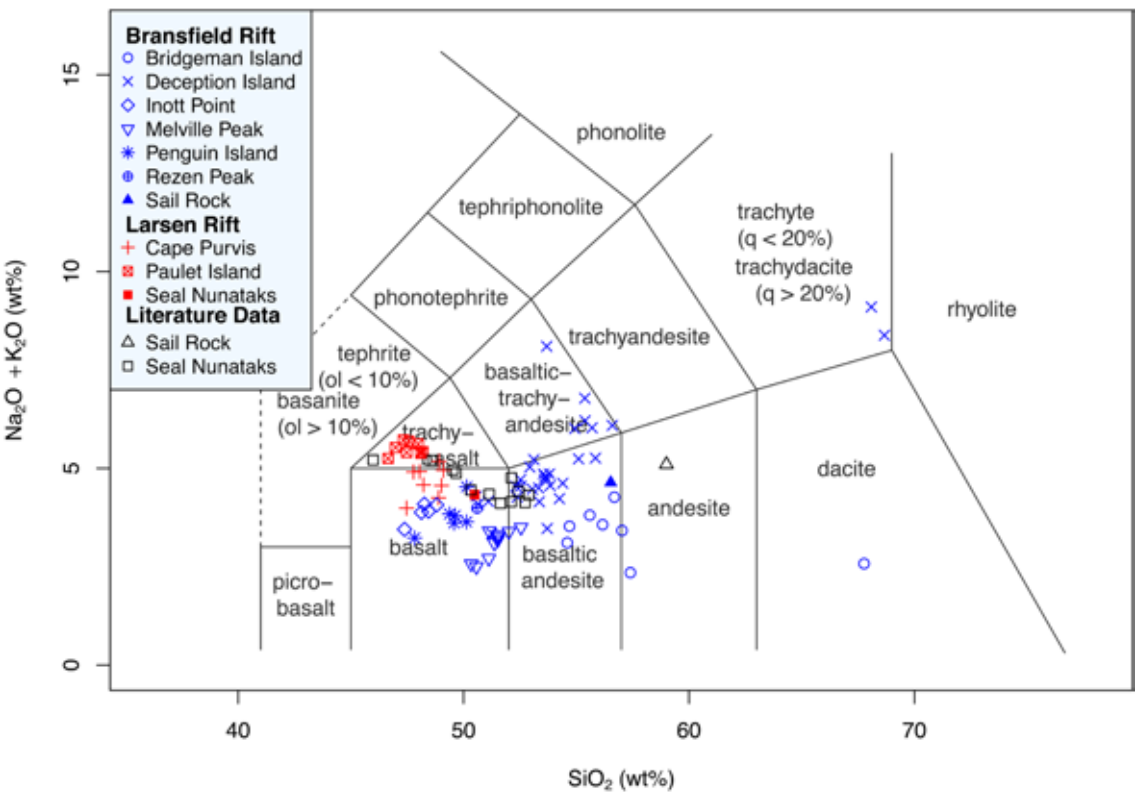

FIG. 11. TAS diagram (after Le Maitre 2002) showing the predominantly basaltic and basaltic andesitic characteristics of the studied volcanic centers. Seal Nunataks literature data taken from Hole (1990) and Hole *et al.* (1993); Sail Rock literature data from Keller *et al.* (1992).

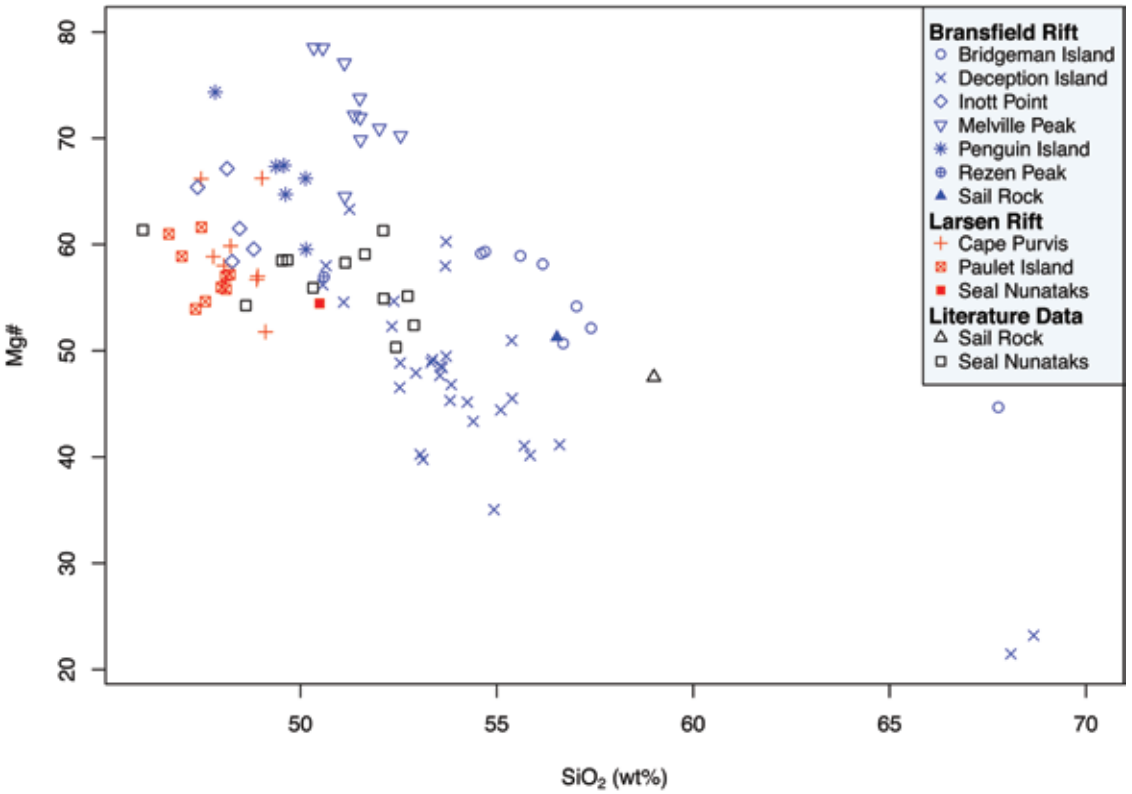

FIG. 12. Using two distinct differentiation indices (SiO_2 *versus* Mg#) reveals that Melville Peak and Paulet Island exhibit the most primitive characteristics of all investigated volcanoes. Melville Peak shows the highest Mg-numbers, Paulet Island the overall lowest SiO_2 contents. Seal Nunataks literature data taken from Hole (1990) and Hole *et al.* (1993); Sail Rock literature data from Keller *et al.* (1992).

dacitic sample from Bridgeman Island (BI-04) was taken from yellowish-reddish lapilli found close to the top of the volcano at approximately 240 m a.s.l., thus rendering unlikely a possible origin from rafted volcanic material originating from somewhere else. This sample yielded, however, a very high LOI (Loss On Ignition) of 8.27 wt%. Consequently, recalculating the bulk rock composition on a volatile-free basis, increased more than anything else its silica content. It is therefore certainly not justified to attribute highly evolved magmas to Bridgeman Island based solely on one strongly hydrated sample.

6.2. Sr-Nd-Pb isotope data

Due to the complicated plate tectonic configuration in the Antarctic Peninsula area, the magma sources of the investigated volcanoes may range from a potentially subduction-influenced back-arc-similar setting in the Bransfield Rift area to an intra-plate setting in the Larsen Rift region.

In order to check for crustal contamination processes and (in the case of the Bransfield Rift volcanoes) for a potentially still detectable signature of subducted sediments, 21 new Sr-Nd-Pb isotope analyses were obtained from Bridgeman Island (3), the Cape Purvis volcano (3), Inott Point (3), Melville Peak (4), Paulet Island (4), Penguin Island (2), Rezen Peak (1) and Sail Rock (1).

Crustal contamination usually occurs during shallow level magma differentiation. Consequently, if such a process takes place, the most differentiated rocks should also be the most contaminated. Thus, plotting isotope data (*e.g.*, εNd) *versus* some differentiation factor (*e.g.*, Mg-number) should display a correlation in case that contamination has occurred (Hildreth *et al.*, 1991; Kraus *et al.*, 2008, 2010). For the investigated volcanoes this is clearly

not the case (Fig. 13), and crustal contamination therefore seems to have been insignificant. This conclusion is furthermore supported by Sr-Nd-Pb isotope data plotting almost entirely within the field occupied by MORB samples dredged from the Drake Passage, not overlapping with Antarctic Peninsula basement or sediments collected from the Drake Passage (Fig. 14).

Particularly in case of the Bransfield Rift volcanoes, a potentially inherited component of subducted sediments in their mantle source could be assumed. However, the vertical trend shown by Sr and Nd isotope data is mostly defined by the Seal Nunataks. This volcanic field is located on the eastern side of the Antarctic Peninsula and associated to the intraplate Larsen Rift. Given the geotectonic setting, we consider an influence of subducted sediments on their mantle source as unlikely. Focusing just on the Bransfield Rift volcanoes, the vertical trend towards Drake Passage sediments is only poorly expressed (Fig. 14A). Moreover, the Bransfield volcanoes plot within the same field as Drake Passage MORB and the latter do also show a vertical trend. Plotting Pb *versus* Nd isotope data (Fig. 14B), our new data do not display any trend towards Drake sediment isotope compositions, supporting the above conclusions.

6.3. Microprobe glass data

Previous studies from other regions (*e.g.*, Stern, 1990, 2008) have shown that the major element compositions of tephra glass may differ strongly from the bulk rock compositions of other volcanic products originating from the same volcanic center and the same eruptive cycle. The reason for this is that the glass represents the last batch of the liquid phase enriched (or depleted) in certain elements, whereas other eruption products (*e.g.*, lava) contain phenocrysts that grew in the magma chamber prior to eruption, thus representing a magma composition at an earlier stage of differentiation.

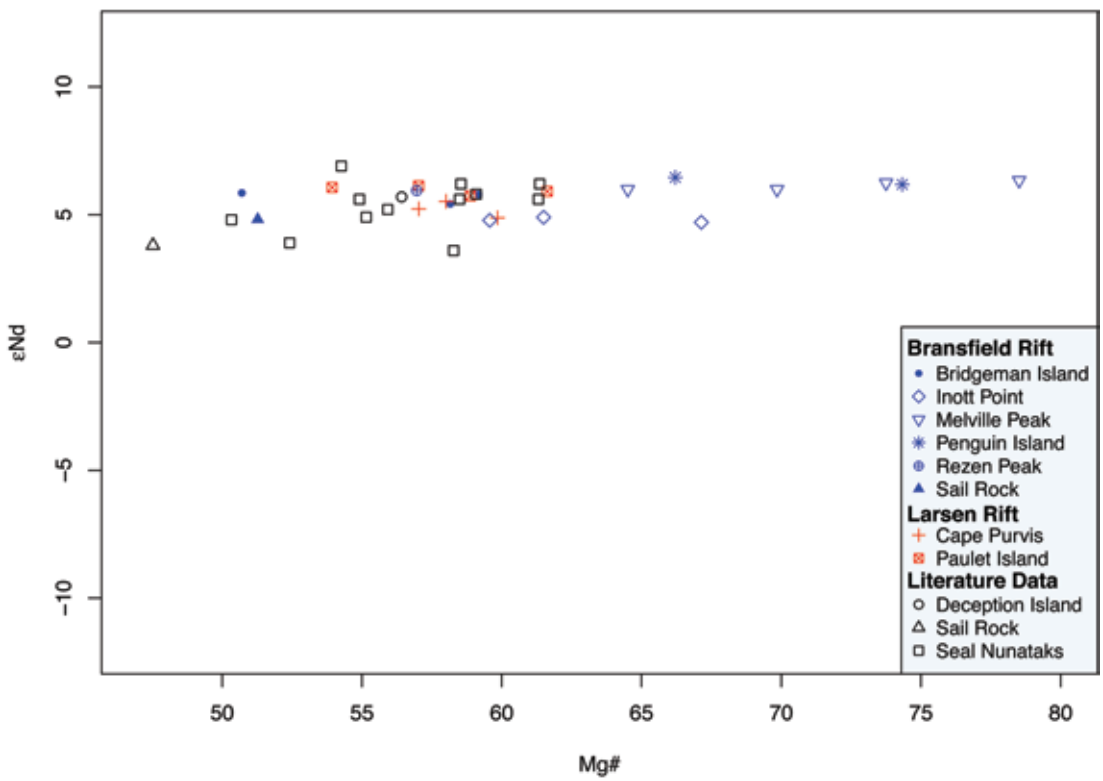

FIG. 13. Plotting Nd isotope data *versus* Mg-number shows no correlation, indicating that no or only insignificant crustal contamination affected the magma differentiation processes and therefore the erupted products. Seal Nunataks literature data taken from Hole (1990) and Hole *et al.* (1993); Sail Rock and Deception Island literature data from Keller *et al.* (1992).

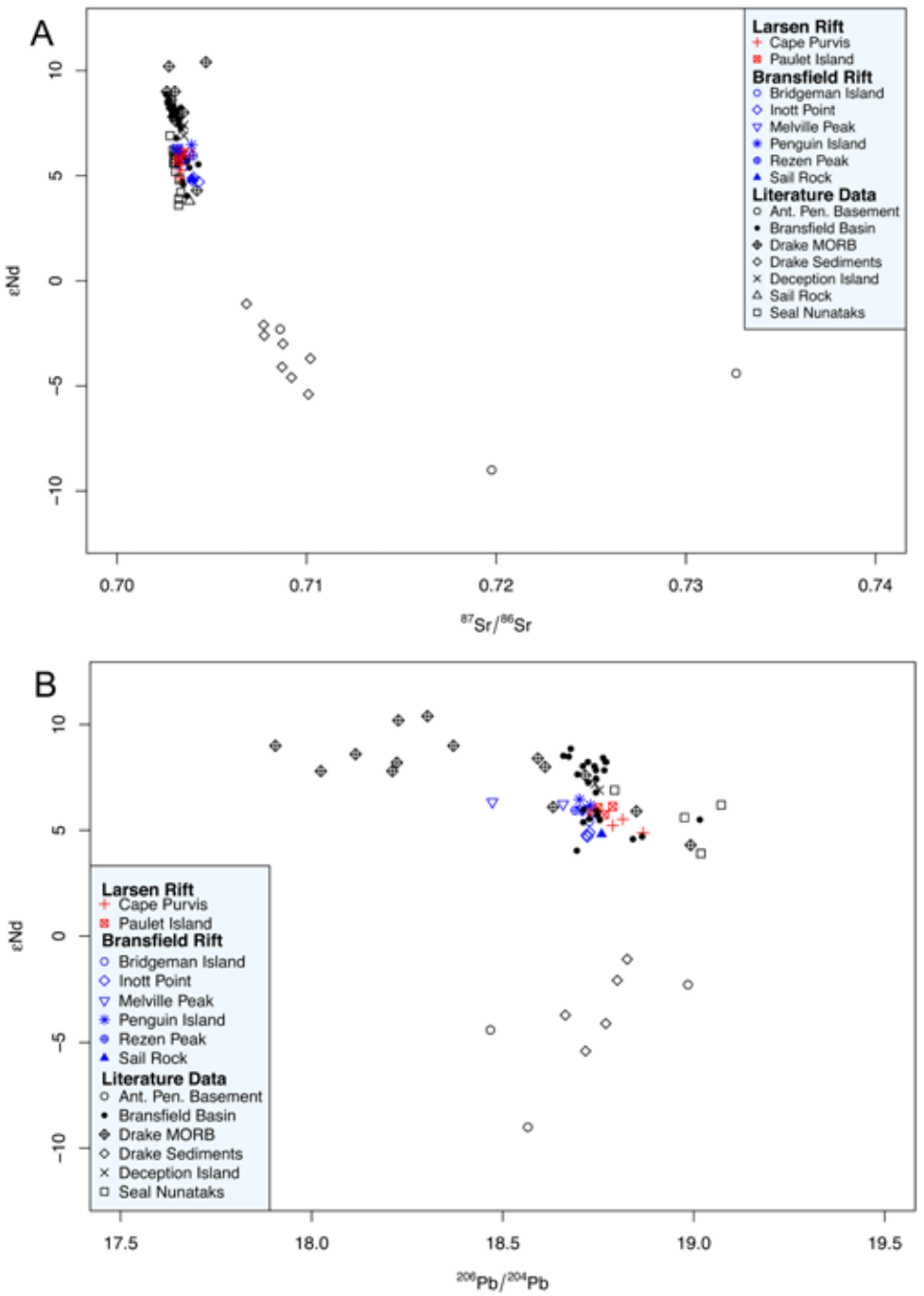

FIG. 14. Plotting Nd *versus* Sr (A) and Pb (B) isotope data gives further evidence that the isotopic composition of the studied volcanoes reflects direct mantle derivates and is not or only very slightly affected by crustal contamination. A sediment component from the formerly active subduction zone beneath the South Shetland arc is also not evident. The volcanoes plot in well-defined clusters within the field occupied by Drake Passage MORB (data from Pearce *et al.* 2001). Seal Nunataks literature data taken from Hole (1990) and Hole *et al.* (1993); Sail Rock and Deception Island literature data from Keller *et al.* (1992). Bransfield Basin seamount data from Keller *et al.* (2002) and Fretzdorff *et al.* (2004). Drake Passage sediment Sr-Nd-data from Walter *et al.* (2000), Drake Passage sediment Pb-data unpublished (courtesy E. Hegner, Univ. Munich, personal communication 2011), Antarctic Peninsula basement data from Millar *et al.* (2001).

Out of 64 samples originally scheduled for microprobe analysis, 43 gave meaningful results (*i.e.*, no reason for sample or analysis rejection, see section 5: methodology), all of them corresponding to hypocrystalline rocks. The remaining 21 samples proved to be holocrystalline and thus devoid of glass (including all Rezen Peak and Sail Rock samples) or yielded too few analyses due to either partial (DI-04A, DI-16A, PI-05) or total (DI-12C) hydration of the glass content.

Comparing the glass compositions with the bulk compositions of the same respective samples, the individual volcanic centers show very different behavior.

A first order observation is that the glass compositions of all volcanoes located along the Bransfield Rift show moderately to strongly increased SiO_2 at only slightly to moderately elevated alkali-contents as compared to the respective bulk compositions (Fig. 15A). In case of Deception Island, a general tendency towards alkali-depletion can be observed. This effect is only slightly expressed or absent in case of basic to intermediate compositions, but more pronounced in case of higher evolved rocks (Fig. 15A). These results could potentially indicate an analytical problem (*e.g.*, alkali-loss due to volatilization effects as a consequence of a too narrow microprobe beam).

However, analyses from the other volcanic centers do not show similar alkali depletion. On the contrary, all other Bransfield Strait volcanoes show moderate alkali enrichment (Fig. 15A) and in case of the Larsen Rift volcanoes, moderate to strong alkali enrichment is observed (Fig. 15B) at identical microprobe conditions, thus contra-indicating analytical problems as source of the trends observed in the Deception Island data. Moreover, studies on inter-microprobe differences of rhyolitic glass analyses found good comparability applying different sets of analytical parameters (Coulter *et al.*, 2010), including also a set of parameters similar to ours (see section 5: methodology).

Specifically the samples from Bridgeman Island show a large shift in silica content; they are of basaltic andesitic bulk, but andesitic to dacitic glass composition (Fig. 15A). Inott Point and Penguin Island volcanoes display a similar increase in SiO_2 as in alkalis, with compositions shifting in both cases from basalt (bulk) to trachybasalt/basaltic trachyandesite (glass).

Sample MP-05B from Melville Peak deserves special attention concerning its glass silica content, displaying an increase of 21.26 wt% as compared to its bulk rock composition (Fig. 15A). The glass compositions of all other samples show SiO_2-values ranging between 1.10 wt% silica-depletion and 12.27 wt% silica-enrichment as compared to the respective bulk rock composition. On average, the glass of the Bransfield Rift volcanoes is 2.88 wt% increased in silica as compared to the respective bulk rock composition (excluding MP-05B from the calculation).

In case of MP-05B, the acquired SEM images and semi-quantitative EDS analyses show that the amount of glass constitutes less than 5% of the sample and its presence is restricted to interstitial areas between silicate minerals. The glass is loaded with small inclusions of iron and titanium rich minerals, possibly magnetite and/or ilmenite. We were able to re-analyze the glass in multiple points without the inclusions. Each point showed high silica values similar to the original microprobe analysis. Its chemistry is far removed from quartz. It is conceivable that it could be some sort of crypto-crystalline amorphous silica-rich alteration, but we could observe no evidence for this. Therefore, we conclude that the high-silica glass composition of MP-05B represents an extreme case of silica enrichment affecting the last batch of the liquid phase.

Rocks from Deception Island show the largest range of values and can roughly be subdivided into three subgroups:

a. A first set of samples shows only very slight variations between bulk and glass compositions; almost all of them are basaltic andesites. These samples were taken from the Baily Head, Fumarole Bay, Stonethrow Ridge and Pendulum Cove formations according to the stratigraphy presented by Smellie (2001).

b. A second set of samples belongs to the Outer Coast Tuff Fm. and displays glass compositions strongly depleted in alkalis but only slightly changed in silica content as compared to the respective bulk compositions.

c. A third sample set was taken from the (stratigraphically youngest) Pendulum Cove Formation and includes the most evolved bulk rock (trachydacite) and glass (rhyolite) compositions. Comparing bulk rock and glass compositions, in this case a notable depletion in alkalis is accompanied by a moderate increase of SiO_2. Given the late

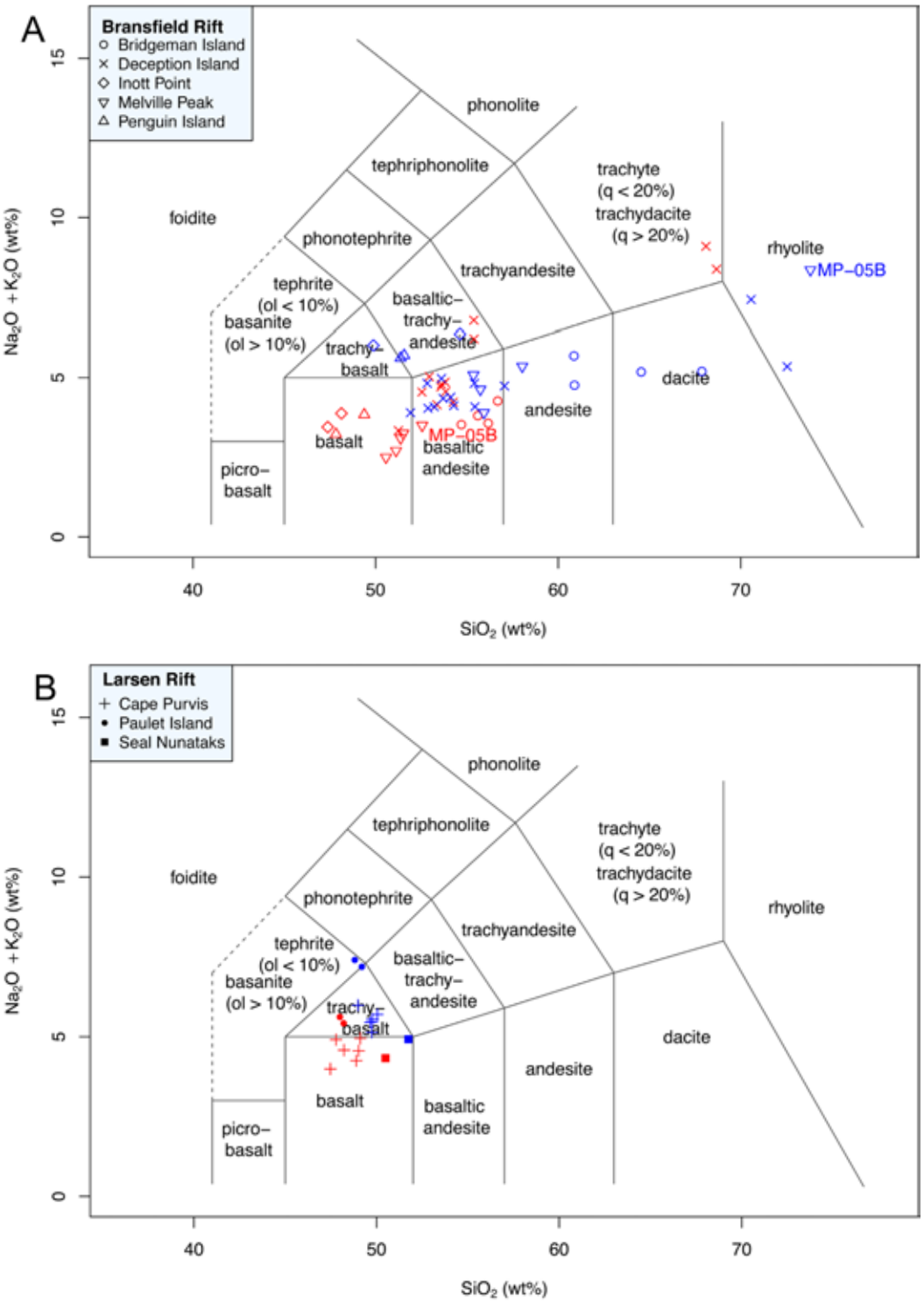

FIG. 15. TAS-diagrams showing bulk rock (ICP-MS; red symbols) plotted *versus* glass compositions (microprobe; blue symbols) of the same respective samples from Bransfield Rift (A) and Larsen Rift (B). Note the different enrichment/depletion behavior of the individual volcanic centers and the generally different tendencies comparing Bransfield Rift and Larsen Rift volcanoes. Sample MP-05B shows an extraordinary strong silica-increase in its glass component.

Holocene and partly even historic age of the Pendulum Cove Formation (Smellie, 2001), in this case alteration processes are unlikely to have caused the alkali depletion of the glass.

It has to be emphasized that with the only exception of the Pendulum Cove Formation, possibly most of Deception Island's stratigraphy is of pre-Holocene age (Smellie, 2001) and that many samples show moderate to advanced states of alteration in thin section, particularly those taken from the Outer Coast Tuff Formation. This implies that at least part of the alkali depletion observed in the glass compositions as compared to the respective bulk rock data could be a result of alteration processes and not primary magmatic features. This would also explain why the samples from the other volcanic centers do not show alkali depletion.

The Larsen Rift volcanoes (Cape Purvis volcano, Paulet Island and the Seal Nunataks) show a different behavior. Without exception, their glass compositions are moderately to strongly increased in alkalis (up to 36%) at only slightly increased silica-contents (Fig. 15B). The glass of the Larsen Rift volcanoes shows an average increase of 1.17 wt% SiO_2 as compared to the respective bulk rock composition. The high alkali contents of their glass component reflect most possibly differentiation processes associated with the intra-plate setting of these volcanic centers. They represent thus a useful tool to distinguish tephra originating from Larsen Rift volcanoes (high total alkalis) from tephra associated with Bransfield Rift volcanoes (low total alkalis).

7. Proposal for a step-by-step identification strategy based on individual geochemical fingerprints

In many diagrams, ICP-MS bulk tephra and lava data together form well defined clusters for most volcanic centers (*e.g.*, Figs. 11, 18), indicating that in these cases the tephra compositions are broadly similar to the lava compositions.

Trace element systematics show that most of the studied volcanic centers appear to have a unique, individual, stable (during the Late Pleistocene-Holocene) and homogeneous upper mantle magma source resulting in tight clustering of the respective data in many diagrams (*e.g.*, Figs. 18, 20). The most pronounced exception to this rule is the Seal Nunataks group, showing a larger spread based on the used literature data (Fig. 20).

In combination with other chemical characteristics, this allows for the geochemical characterization of the individual volcanoes by combining the information given by different chemical elements or element ratios (Fig. 16), holding especially true for trace and rare earth element ratios. In the following, we will present a step-by-step strategy based on the characteristic chemical features of each individual volcanic center, yielding a high potential to correctly identify the source of a distal tephra layer of unknown origin, if it was produced by one of the investigated volcanic centers.

7.1. Step 1: Distinction between Larsen Rift and Bransfield Rift volcanoes

The Larsen Rift volcanoes are associated with an intra-plate geotectonic setting, while the Bransfield Rift volcanic centers belong to a marginal basin with a back-arc character (*e.g.*, Hole, 1990; Keller *et al.*, 1992, 2002). Consequently, the Larsen Rift volcanoes tend towards alkali basaltic compositions while the volcanoes located along Bransfield Rift belong to the subalkali series. In terms of major element compositions, this is reflected by the up to 4.5 times higher K_2O content of the Larsen Rift volcanoes; the data display contents generally higher than 1 wt% for the Cape Purvis volcano, Paulet Island and some of the Seal Nunataks centers, while the Bransfield Rift volcanoes in general have K_2O <1 wt% (Fig. 17).

Only two trachydacites and one basaltic trachyandesite sample from Deception Island have equal or even slightly higher potassium contents than the Larsen Rift volcanoes. The exception to this pattern is the Seal Nunataks group, which predominantly plot at the upper limit of the Bransfield Rift values at <1 wt% K_2O (Fig. 17), and only about 30% of them well within the field occupied by the other Larsen Rift volcanoes. Despite the different applied analytical techniques (ICP-MS in our case, XRF and INAA in case of the literature data taken from Hole (1990) and Hole *et al.* (1993)), we consider these values more likely to reflect true compositional spread than an analytical artifact. In fact, Hole (1990) reports for the Seal Nunataks a compositional spread ranging from alkali via transitional basalts to olivine and quartz tholeiites, with the latter having K_2O contents well below 1 wt%. This is consistent with the K_2O-pattern shown by our new data.

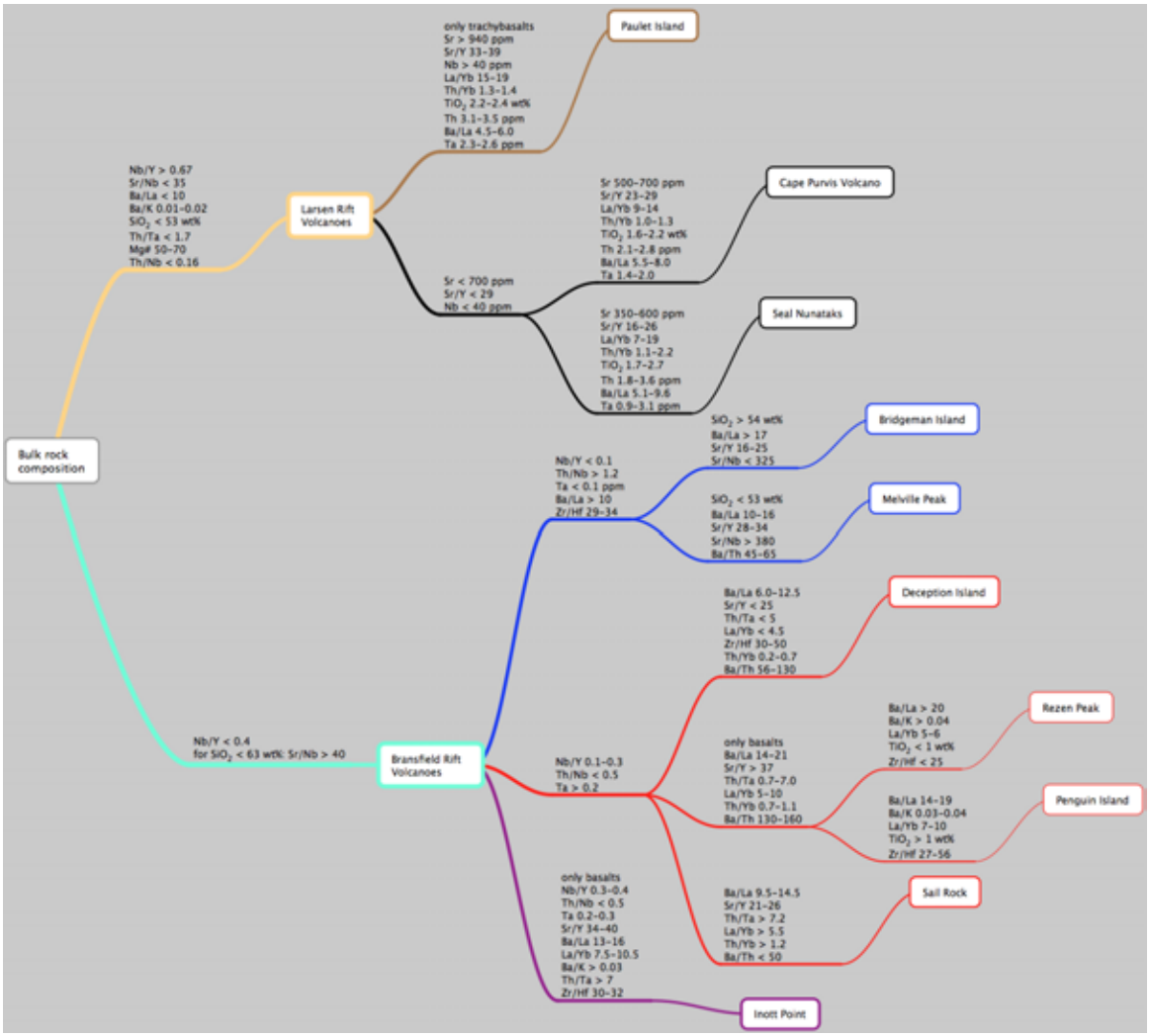

FIG. 16. The 'Decision Tree', a flow chart that we propose as a new step-by-step strategy to identify the source volcano of a distal tephra layer of unknown origin. The approach is based on geographically zooming in onto the most likely source volcano, as a first step distinguishing between Bransfield Rift and Larsen Rift volcanoes and then refining within the respective group of volcanoes. It is important to note that none of the indicated geochemical characteristics alone is diagnostic, but that the combined chain of geochemical conditions leading to a specific volcano yields a very high potential of identifying it correctly as source of a tephra layer of unknown origin.

More convincing is the pattern shown by immobile trace elements. Using the Nb/Y ratio as an indicator of alkalinity, the Larsen Rift volcanoes display values up to an order of magnitude higher than the volcanic centers associated with the Bransfield Rift (Fig. 18). This condition is met by all samples, including the three trachytic samples from Deception Island that in figure 17 plot at high K_2O values within the Larsen Rift range.

Another characteristic feature of the Larsen Rift volcanoes related to potassium is the restriction of their Ba/K ratios to the very narrow range of 0.01-0.02 (Fig. 19). The Larsen Rift volcanoes plot along a horizontal trend line characterized by variable Nb/Y but uniform Ba/K ratios. The Bransfield Rift group shows the contrary behavior, plotting along a vertical trend line of varying Ba/K but fairly uniform Nb/Y (Fig. 19). These relations are independent of silica

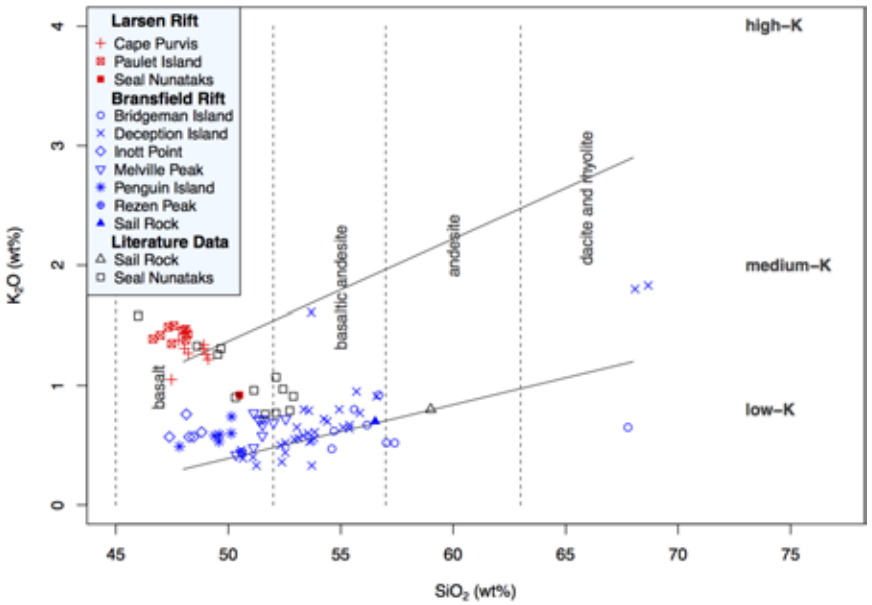

FIG. 17. Degree of alkalinity as reflected by the K_2O content plotted against SiO_2. Seal Nunataks literature data taken from Hole (1990) and Hole *et al.* (1993); Sail Rock literature data from Keller *et al.* (1992).

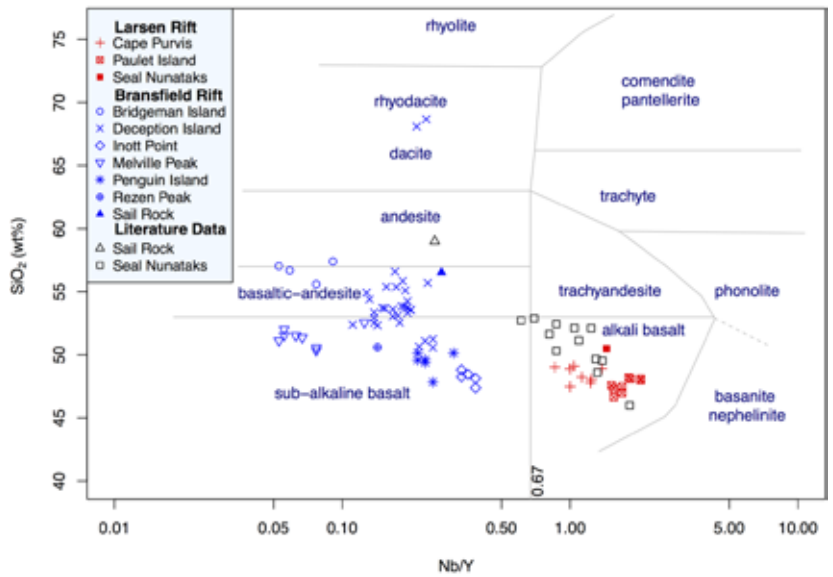

FIG. 18. Determination of magma series and rock type classification using SiO_2 as differentiation index and the Nb/Y ratio as indicator of alkalinity (modified after Winchester and Floyd, 1977). Note the clear separation between Larsen Rift and Bransfield Rift volcanoes corresponding to their respective geotectonic setting, and the tight clustering of the individual volcanic centers showing little or no overlap. Note also, that some samples (*e.g.*, the high-silica sample from Bridgeman Island, BI-04) do not plot in this diagram because their Nb values are below the ICP-MS detection limit. Except for the dacite/rhyolite-boundary, all other, horizontal (SiO_2-content defined) boundaries from the original diagram delimiting the fields of the subalkali-series have been replaced with the now widely accepted SiO_2-boundaries used in the total alkali-silica-diagram (TAS; Le Maitre, 2002). The (sub-) vertical boundaries and the boundaries delimiting the fields of the alkali-series correspond to the original diagram published by Winchester and Floyd (1977). Seal Nunataks literature data taken from Hole (1990) and Hole *et al.* (1993); Sail Rock literature data from Keller *et al.* (1992).

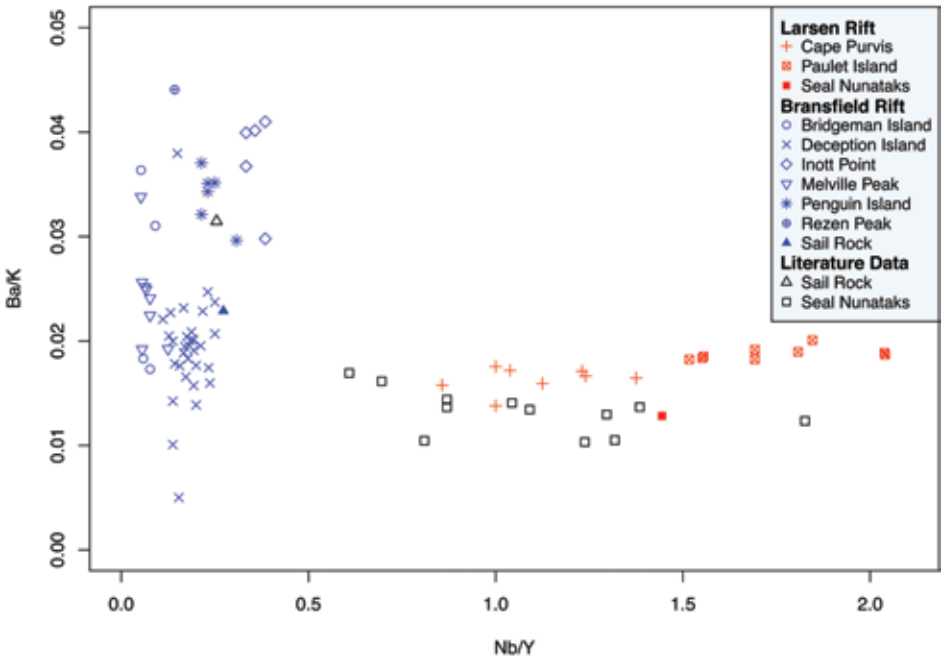

FIG. 19. Different trend behavior of Bransfield Rift and Larsen Rift volcanoes: while the former show vertical trends along varying Ba/K ratios but at rather uniform Nb/Y, the latter display horizontal trends along varying Nb/Y at fairly uniform Ba/K. Elemental K was calculated using the formula $K=K_2O$ *0.83014778*10000. Seal Nunataks literature data taken from Hole (1990) and Hole *et al.* (1993); Sail Rock literature data from Keller *et al.* (1992).

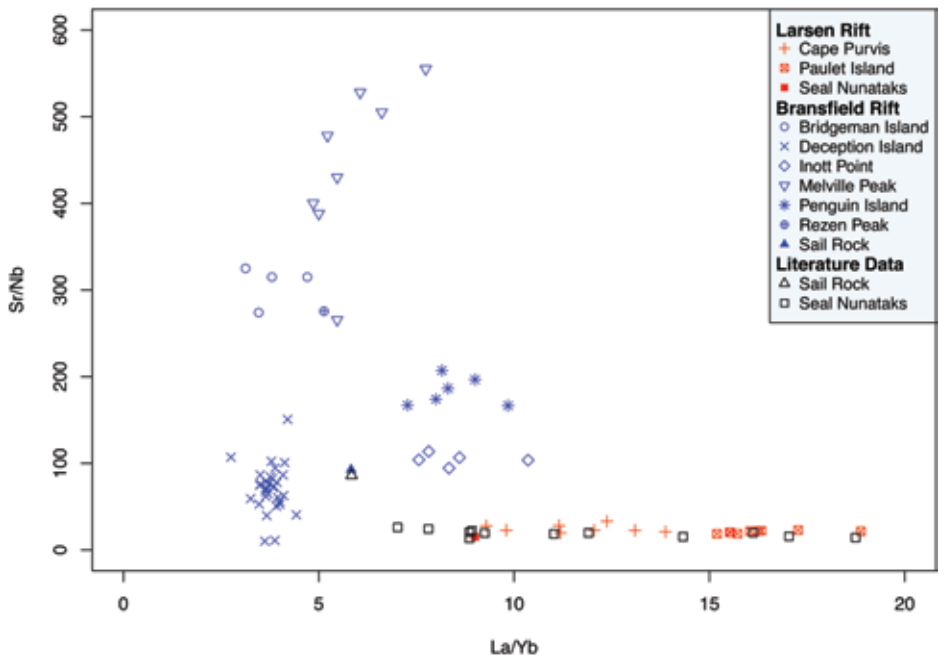

FIG. 20. Trace and rare earth element ratios characterizing and separating the individual volcanic centers from each other. While the Larsen Rift group plots along horizontal trends towards elevated La/Yb but at uniform Sr/Nb ratios, most of the Bransfield Rift volcanoes cluster tightly. Seal Nunataks literature data taken from Hole (1990) and Hole *et al.* (1993); Sail Rock literature data from Keller *et al.* (1992).

content, and therefore fractionation. A similar pattern is observed when plotting La/Yb *versus* Sr/Nb (Fig. 20). While the Larsen Rift volcanoes plot strictly along a horizontal trend defined by variable La/Yb but uniform Sr/Nb ratios lower than 35, the Bransfield Rift volcanoes show either well-defined clustering (Deception Island, Inott Point, Penguin Island, Bridgeman Island, Sail Rock) or a steep trend of increasing Sr/Nb at only slightly increasing La/Yb (Melville Peak).

Other compositional conditions generally met by the Larsen Rift group are SiO_2 <53 wt% (Fig. 11), Mg-numbers between 50 and 70 (Fig. 12), Ba/La <10 (Fig. 22A), Th/Nb <0.16 and Th/Ta <1.7 (Fig. 16). For the Bransfield Rift group, only one universally valid geochemical condition could be identified that delimits all samples within a narrow range: Nb/Y ratios lower than 0.4 (Figs. 16, 18). A second condition characteristic for this group (Sr/Nb ratios higher than 40; Fig. 20) applies only for samples with SiO_2 <63 wt%, hence excluding more evolved rocks.

7.2. Step 2: Distinction within the Larsen Rift group

Based on TAS major element chemistry, a first order observation is that all samples from Paulet Island are trachybasalts, while all but one sample from Cape Purvis and most from the Seal Nunataks are basalts and basaltic andesites (Fig. 11). The only exceptions to this pattern are sample CP-03 (a trachybasaltic lava from Cape Purvis that might have undergone some K- or Na-enrichment due to post-magmatic alteration processes) and two samples from the Seal Nunataks taken from the literature (Hole *et al.*, 1993).

Smellie *et al.* (2006a, b) state a strong compositional similarity between Paulet Island and the Cape Purvis volcano based on major elements only. Such a similarity, however, is not evident from the trace and rare earth element data now available.

7.2.1. Paulet Island

The most pronounced compositional features distinguishing Paulet Island from the Cape Purvis volcano and the Seal Nunataks are Sr/Y >33 (Fig. 22A), La/Yb >15 (Fig. 20), Ta >2.3 ppm, and very high Sr values (>940 ppm). No other volcano (including those of Bransfield Rift) displays such high Sr contents, making it a unique and diagnostic feature of Paulet Island. Because Paulet Island also shows the highest Nb-contents, its Sr/Nb ratios fall in the same narrow range as those of Cape Purvis and the Seal Nunataks (Fig. 20).

The reasons for Paulet Island's conspicuous features may be:

a. A very inhomogeneous mantle source beneath Larsen Rift even at short distances (only 10 km distance between Paulet Island and Cape Purvis). A possible small-scale heterogeneity of the asthenosphere beneath the Antarctic Peninsula has also been stated by Hole *et al.* (1993).

b. A smaller degree of partial melting for Paulet Island magmas. Apart from the geochemical indications, the much smaller size and volume of Paulet Island's volcanic edifice as compared to the Cape Purvis volcano - despite similar timing of initial activity (Late Pleistocene: Rex, 1976; Smellie *et al.*, 2006a, b) - support this conclusion.

7.2.2. Cape Purvis volcano and Seal Nunataks

The distinction between the Cape Purvis volcano and the Seal Nunataks is less clear. The Seal Nunataks have Sr contents of 350-600 ppm (Cape Purvis: 500-700 ppm), but a pronounced compositional gap like the one separating those two volcanic centers from Paulet Island (Fig. 22A) does not exist. The compositional gap between Paulet Island plotting at high La/Yb and Cape Purvis and Seal Nunataks at lower values as indicated by our new data, is not supported by literature data from the Seal Nunataks plotting partly well within the field occupied by Paulet Island (Fig. 20). However, the Seal Nunataks tend towards lower Sr/Y ratios (16-26) as compared to the Cape Purvis volcano (23-29), and to higher Th/Yb (1.1-2.2 and 1.0-1.3, respectively).

Generally, the Seal Nunataks compositional variability is much larger than that of the Cape Purvis volcano, and many geochemical features defining the Cape Purvis volcano's composition within narrow limits (La/Yb, Th and Ta contents, Ba/La, Fig. 16) fall well within the ranges covered by the Seal Nunataks. It has to be emphasized, however, that the Seal Nunataks are a volcanic field comprising 16 individual volcanoes with chemical compositions ranging from tholeiites to alkali basalts (Hole, 1990), while the Cape Purvis volcano is a single volcanic edifice; hence a smaller geochemical variability has to be expected in case of the latter.

7.3. Step 3: Distinction within the Bransfield Rift group

A clear geochemical distinction within this group is more complicated due to the higher number of volcanoes associated to this rift system (Fig. 16). The Bransfield Rift volcanoes can roughly be subdivided into three subgroups of similar chemical composition:

- Melville Peak and Bridgeman Island,
- Deception Island, Rezen Peak, Penguin Island and Sail Rock,
- Inott Point.

7.3.1. Melville Peak and Bridgeman Island

Again, the Nb/Y ratio gives a first indication. Of all studied volcanoes, only Melville Peak and Bridgeman Island show Nb/Y ratios lower than 0.1 (Fig. 21), the only exception to this pattern being one sample from Melville Peak (MP-05B, tephra: Nb/Y = 0.13). Deception Island, Rezen Peak, Penguin Island and Sail Rock have Nb/Y values between 0.1 and 0.3, while Inott Point displays ratios between 0.3 and 0.4 (Figs. 18, 21). Another diagnostic feature that clearly distinguishes Melville Peak and Bridgeman Island from the other volcanoes is their very high Th/Nb ratio (>1.2). All other volcanoes have Th/Nb ratios lower than 0.5, including those from Larsen Rift (Fig. 16). A similar pattern applies concerning the Zr/Nb ratio. Moreover, Melville Peak and Bridgeman Island are the only volcanoes having Ta contents generally below ICP-MS detection limit (< 0.1 ppm). Among the analyzed samples there is no exception to this rule.

To distinguish between Melville Peak and Bridgeman Island, a first hint is given by SiO_2-contents and Ba/La ratios. While Melville Peak samples plot tightly clustered at SiO_2=50-53 wt% and Ba/La=10-16, Bridgeman Island's lithologies are more evolved (SiO_2= 54-68 wt%) at Ba/La ratios >17. Furthermore, all but one sample from Bridgeman Island have Sr/Y ratios <25, while Melville Peak samples plot at Sr/Y ratios between 28 and 34 (Fig. 22B). Again, Melville Peak shows tight clustering while Bridgeman Island spreads over a larger range.

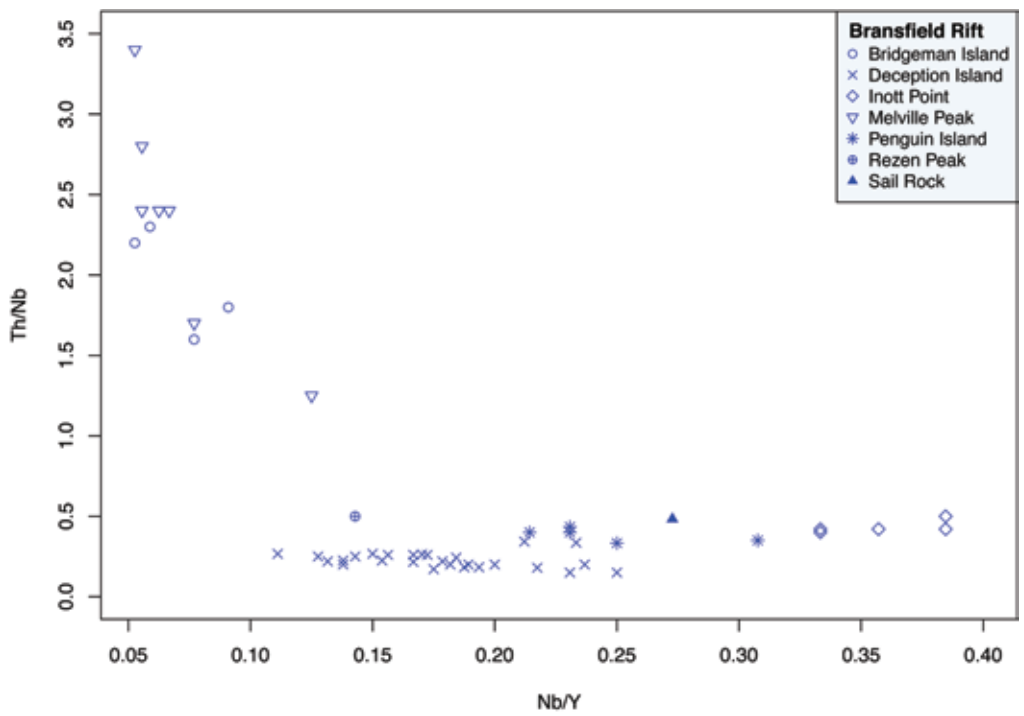

FIG. 21. Trace element systematics within the Bransfield Rift volcano group. While Melville Peak and Bridgeman Island show higher Th/Nb and lower Nb/Y ratios than any other volcano, Inott Point is the only one displaying Nb/Y ratios in the range 0.33-0.38. The Larsen Rift volcanoes are omitted from this diagram; they plot at Nb/Y ratios higher than 0.67.

This effect is most possibly related to differences in the respective differentiation processes, as confirmed by the high Mg-numbers displayed by Melville Peak indicating rapid magma ascent and short storage times in a shallow level magma chamber and the higher SiO_2-contents of Bridgeman Island samples indicating a higher degree of differentiation (Figs. 11, 12). In terms of Sr/Nb, Melville Peak tends to values higher than 400, while Bridgeman Island is clustering around 300 (Fig. 20).

7.3.2. Deception Island, Rezen Peak, Penguin Island and Sail Rock

Subdivision between the four volcanoes of this group does not become clear from only one geochemical feature. Instead, a combination of chemical conditions must be checked (Figs. 16, 22B).

All volcanoes of this subgroup are characterized by Nb/Y ratios between 0.1 and 0.3, Th/Nb <0.5, and Ta contents between 0.2 and 1.3 ppm.

To distinguish Deception Island from the much smaller, close-by situated Sail Rock volcano, both Th/Ta as well as La/Yb prove useful. While Deception Island has Th/Ta <5 and La/Yb <4.5, Sail Rock displays Th/Ta >7 and La/Yb >5.5 (Fig. 20).

The distinction between Deception Island and the subgroup Rezen Peak / Penguin Island (Fig. 16) is well constrained: Deception Island samples have Ba/La ratios below 12.5, while the other two volcanoes show without exception Ba/La >14 (Fig. 22B). Furthermore, Deception Island's Sr/Y is lower than 25 while Rezen Peak and Penguin Island have Sr/Y >37. Like in the case of Sail Rock, Rezen Peak and Penguin Island both have La/Yb >5 while Deception Island's values are below 4.5.

Concerning the distinction between Rezen Peak and Penguin Island, Rezen Peak shows very high Ba/La ratios (>20) while Penguin Island's values range between 14 and 19 (Fig. 22B). Another striking difference is the La/Yb ratio, Rezen Peak plotting at 5.1 while the Penguin Island samples have ratios higher than 7.2 (Fig. 20). Rezen Peak is also the volcano with the lowest Zr/Hf (24.7). All other volcanoes show Zr/Hf >30, the exception to this rule being only two samples from Penguin and Bridgeman Island (PI-01 and BI-07, respectively) that have Zr/Hf between 27.5 and 29. The Ba/La and Sr/Y ratios (Fig. 22B) as well as Th/Ta can be used to distinguish the Rezen Peak/Penguin Island subgroup from Sail Rock.

7.3.3. Inott Point

This volcanic center is name-giving for the Inott Point Formation introduced by Smellie *et al.* (1995, 1996). All analyzed samples are of basaltic TAS geochemistry. This is the only volcano featuring Nb/Y ratios ranging from 0.33 to 0.38 (Fig. 21). None of its other geochemical characteristics (Fig. 16) is unique and therefore diagnostic for this volcano, but combining the information given by Th/Nb, La/Yb, Ba/La, Ba/K and Th/Ta ratios proves useful to unequivocally characterize its eruptive products.

8. Application of the proposed strategy and correlation with published data

The comprehensive database for Late Pleistocene-Holocene tephra from northern Antarctic Peninsula volcanic centers allows correlation of the resulting data with published data from ice cores (*e.g.*, Aristarain and Delmas, 1998), lake sediments (*e.g.*, Björck 1991a, b, c, 1993) and marine sediment cores (*e.g.*, Hubberten *et al.*, 1991; Fretzdorff and Smellie, 2002).

In the near future, the project "Climate of the Antarctic and South America (CASA): Joint Brazilian-Chilean-US ice core drilling on the Detroit Plateau, Antarctic Peninsula" will generate additional important new ice core data (possibly including tephra layer analyses) from the northern Antarctic Peninsula that shall be merged and correlated with the data presented here.

8.1. Application of the proposed strategy - Revealing the origin of Livingston Island ice tephras

During austral summer 2008/2009, a sequence of 10 tephra layers incorporated in the ice cap of Livingston Island was observed in the area of Perunika Glacier (Hurd Peninsula, central Livingston Island). The lowermost eight of them are evident at the fast-flowing front of Perunika Glacier (Fig. 23), while the uppermost two are intersecting with the glacier's surface close to the edge of the ice cliff. Most of these volcanic ash horizons are possibly the same as those studied in a previous work at some 5 km distance at Johnson's Dock and other localities in central Livingston Island (Pallás *et al.*, 2001). This is suggested by the distinctive distribution pattern of the tephra layers, comprising a bundle of six lower layers (bundle 3), followed about 10 m higher by an intermediate

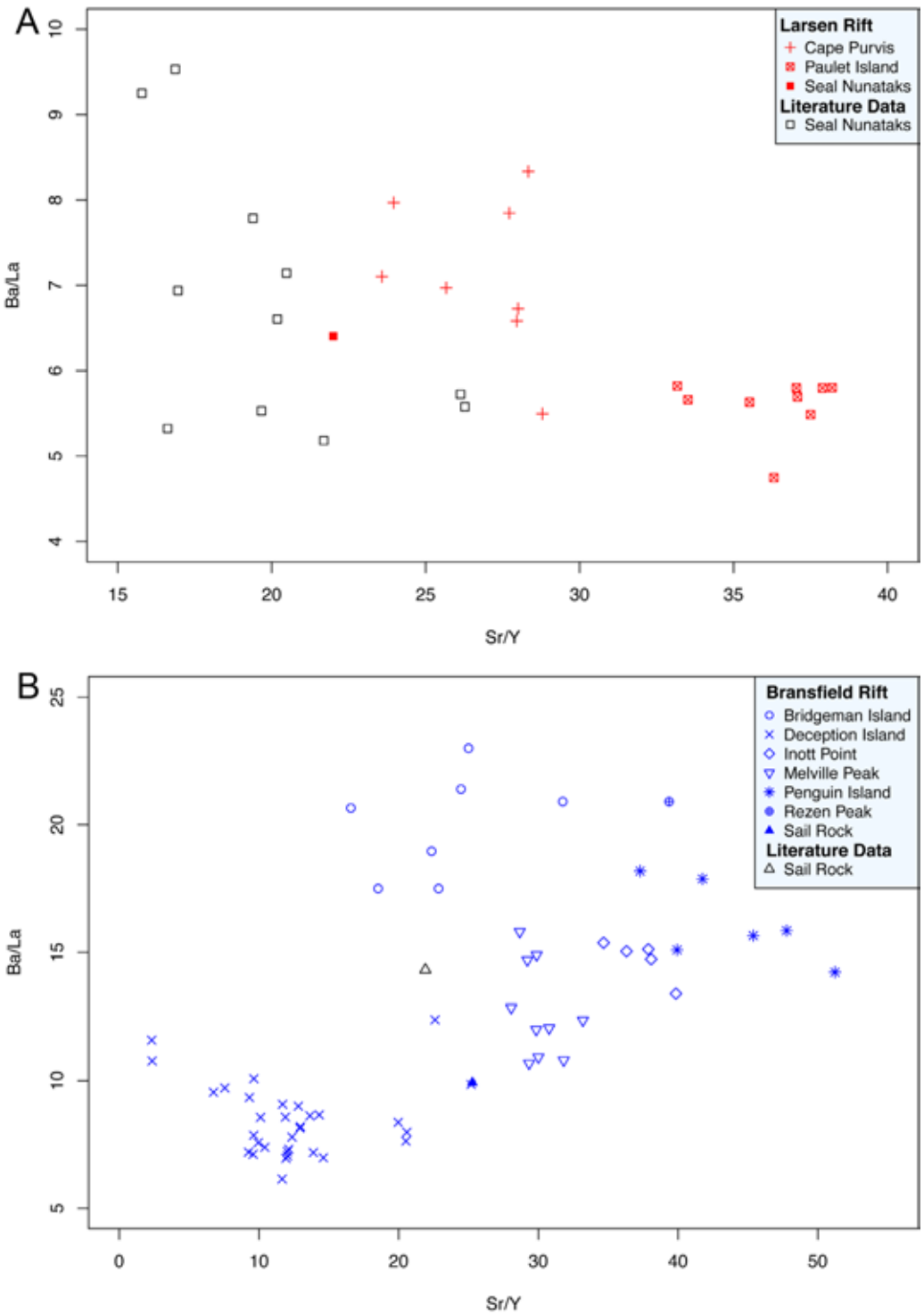

FIG. 22. Ba/La *versus* Sr/Y ratios of Larsen Rift (A) and Bransfield Rift (B). Larsen Rift in general has very low Ba/La values as compared to Bransfield Rift. Note the pronounced gap separating Paulet Island from the other Larsen Rift volcanoes. Concerning Bransfield Rift (B), clustering of the individual volcanoes reflects compositional differences. Seal Nunataks literature data taken from Hole (1990) and Hole *et al.* (1993); Sail Rock literature data from Keller *et al.* (1992).

double layer (bundle 2) and further 6 m higher by another double layer (bundle 1; cf. figure 23 (this paper) and figure 3 in Pallás *et al.*, 2001). The lower bundle of six layers at Perunika Glacier is possibly the same as the one Pallás *et al.* (2001) termed TPH3 at Johnson's Dock. The intermediate double layer observed at Perunika Glacier therefore likely corresponds to the TPH2 bundle reported by those authors, and the highest double layer to their uppermost TPH1 horizon. However, while Pallás *et al.* (2001) describe TPH1 as comprising only one single tephra layer, at Perunika glacier it consists clearly of two distinct layers. Pallás *et al.* (2001) attributed all tephra layers to Deception Island.

In order to check if the here presented step-by-step strategy (Fig. 16) actually works, we sampled nine of the ten tephra layers at different locations of Perunika Glacier (17 samples in total). Only the lowermost layer remained inaccessible due to outcrop conditions. We determined the stratigraphic position of each layer and therefore the relative age relationships. The tephra horizons were sampled at a steeply inclined part of the Perunika Glacier close to the front by removing about 0.5-1.0 m^2 of the ice roof above each tephra layer in order to expose the volcanic ash, while avoiding contamination with tephra washed down from higher situated layers. The thus exposed tephra was then sampled from the surface below the removed roof using the broad side of an ice axe, avoiding the outer border zones where contamination by ash washed down from above might have occurred.

All tephra layers consist predominantly of black and subordinately (<10%) of red components. The topmost layer 1 is very fine grained (<0.1 mm) as compared to the others (usually featuring grain sizes up to 1 mm). Layer 7, one of the six layers of bundle 3 at the bottom of the sequence, is similarly fine-grained as layer 1 and very thin (<0.5 mm), making it difficult to recover sufficient sample material even from an area of about 1 m^2.

The position of the ice tephras within the glacier is not uniform. Instead, the individual layers bend upwards towards both sides of the ice cliff shown in figure 23 and intersect with the glacier surface at different altitudes above sea level. This reflects not only intra-glacial deformation processes but also the velocity of the ice flow, being highest in the center of the section. Here, older ice originally located beneath the tephra layers has already been discharged into the sea, dragging the volcanic ash horizons down to sea level. Laterally, towards both sides of the ice cliff, the ice flow velocity is slower. Thus, the amount of older ice beneath the tephra layers rises with distance from the fastest flowing part of Perunika Glacier, as reflected by the ash layers bending upwards and intersecting with the glacier surface at successively higher altitudes above sea level and at larger distances from the shoreline.

We conclude that careful three-dimensional mapping of the intersection lines of the tephra horizons with the surface of the ice cap could reveal a precise picture of ice flow velocities, ice thicknesses and intra-glacial deformation processes. The ice along the beach further away from Perunika Glacier Cove appears to be devoid of ash layers. The sequence of 10 layers observed at Perunika Glacier could thus be the most complete tephra sequence in central Livingston Island.

FIG. 23. Location and outcrop situation of ice tephras at Perunika Glacier in central Livingston Island (view towards SE). The entire sequence comprises ten different volcanic ash layers, subdivided into three separate bundles. The upper two bundles (1 and 2) comprise two layers each; bundle 3 at the bottom consists of six layers. The application of our proposed step-by-step flow chart identifies Deception Island unequivocally as source volcano of all nine sampled ice tephra horizons. Only the bottommost layer of bundle 3 remained inaccessible. Note the lateral upward bending of the ash layers, indicating lower ice flow velocities in those areas as compared to the central part of the section.

Applying the step-by-step strategy illustrated in figure 16, the ice tephras are first plotted into a Nb/Y-SiO_2 classification diagram like the one shown in figure 18, revealing that all of them are basaltic andesites and andesites with Nb/Y ratios between 0.16 and 0.27. Furthermore, they feature Sr/Nb ratios ranging from 39.8 to 79.2, making it safe to assume that they originated from one of the Bransfield Rift volcanoes and not from Larsen Rift.

In a second step, their range of Nb/Y ratios in combination with Th/Nb ratios below 0.5 leads to the subgroup consisting of Deception Island, Rezen Peak, Penguin Island and Sail Rock (Fig. 16).

In a final step, the ice tephras' Ba/La ratios ranging from 8.3 to 10.7 in combination with Sr/Y<15 (both conditions ruling out Rezen Peak and Penguin Island), Th/Ta<4 (excluding Sail Rock) and La/Yb ≤4.5 (only fitting Deception Island) identify Deception Island unequivocally as their source volcano. A La/Yb *versus* Sr/Nb plot visualizes convincingly that the Livingston Island ice tephras plot entirely within the field occupied by samples from Deception Island but well outside the field of all other investigated volcanoes (Fig. 24). Besides confirming the conclusion of Pallás *et al.* (2001) that all tephra layers in central Livingston Island originated from Deception Island, these data also convincingly show that the step-by-step pattern illustrated in figure 16 works reliably.

8.2. Development of tephra databases and the impact on paleoclimate research

Modern paleoclimate research is heavily dependent on establishing accurate timing related to rapid shifts in Earth's climate, with the aim of correlating these events at local to global scales to assess phasing of climate variability for different parts of the globe. Volcanic ash (tephra) has a demonstrated importance in correlating local and global sedimentological

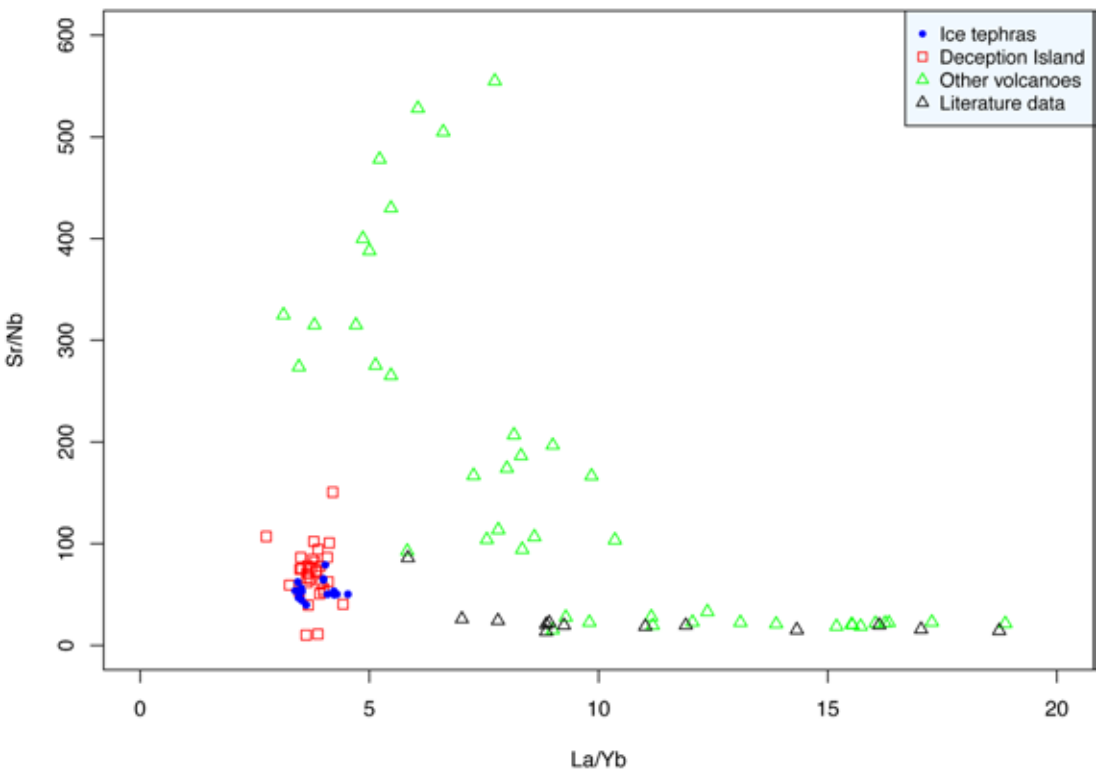

FIG. 24. La/Yb *versus* Sr/Nb demonstrating that the Livingston Island ice tephras plot entirely within the field occupied by samples from Deception Island, not overlapping with other volcanic centers. Seal Nunataks literature data taken from Hole (1990) and Hole *et al.* (1993); Sail Rock literature data from Keller *et al.* (1992).

deposits (Alloway *et al.*, 2007; Pearce *et al.*, 2007; Lowe, 2008, 2011). However, not every volcanic center or volcanic eruption creates globally distributed tephra layers. Several regional tephrochronological frameworks have been established in the last decade, *e.g.*, for Europe (Turney *et al.*, 2004; Newton *et al.*, 2007; Lane *et al.*, 2011, 2012) and New Zealand (Alloway *et al.*, 2007), as well as some databases that include a wider variety of volcanic and igneous rocks. A number of regional database projects, including Tephrabase, NAVDAT, Central Andes, GeoMapApp, and GEOROC, implement data storage and availability for specific geographical regions.

Once tephra is detected in a paleoclimate archive, the composition of the unknown tephra layer must be quantitatively compared to that of known eruptions in order to identify its source. The most effective tool for these comparisons is a comprehensive geochemical and geochronological database, containing high quality, reviewed geochemical and geochronological data, as well as statistical tools for evaluating geochemical similarities.

The location and identification of tephra in ice cores raises the significance of the volcanic records available therein to much greater levels. Determining the source volcano of the tephra, through matching the chemistry of the volcanic glass found in the ice core with that from the particular eruption (*e.g.*, De Angelis *et al.*, 1985; Palais *et al.*, 1992; Zielinski *et al.*, 1997; Narcisi *et al.*, 2010a, b; Dunbar and Kurbatov, 2011), can also tie the volcanic aerosol signal to a specific eruption. The ability to reliably identify the eruption(s) responsible for a particular signal provides the information needed to clearly assess the climatic forcing capability of a particular eruption/volcano and of a particular type of eruption, *e.g.*, a plinian *versus* fissure type of eruption, or tropical *versus* high latitude.

8.3. Availability of other published data

Among the at least 12 volcanic centers in the northern Antarctic Peninsula area that are known or suspected to have shown Late Pleistocene-Holocene explosive activity (Fig. 1), only Deception Island has so far been confirmed as source for tephra particles or sulfate identified in a number of Antarctic ice cores (Delmas *et al.*, 1992; Aristarain and Delmas, 1998; Han *et al.*, 1999; Karlof *et al.*, 2000; Pallás *et al.*, 2001; Budner and Cole Dai, 2003) and lake records (*e.g.*, Björck *et al.*, 1991a, b). Tephra particles and sulphate from Deception Island have been transported as far as the South Pole (*e.g.*, Budner and Cole-Dai, 2003) and were produced by eruptions that occurred during the last 500 years, belonging to an evolutionary phase that is characterized by only small to moderate volume eruptions (Smellie, 2001). If, however, small to moderate volume eruptions from Deception Island were capable of distributing tephra to large distances, the same should be possible for other volcanic centers that have not shown major volcanic eruptions so far. Other volcanic centers with highly likely Holocene activity are Penguin Island and the Seal Nunataks. Furthermore, Brabant Island, Sail Rock, Inott Point, Edinburgh Hill, Melville Peak, Bridgeman Island, the Cape Purvis volcano, Paulet Island and eastern James Ross Island (Fig. 1) are likely to have been active during Late Pleistocene-Holocene times (*e.g.*, González-Ferrán, 1983, 1995; Smellie, 1990; Smellie *et al.*, 1995, 1996, 2006b, 2008).

Deception Island has been studied in detail and numerous analytical data are available for lava, bombs and dikes (Hawkes, 1961; González-Ferrán and Katsui, 1970; Valenzuela *et al.*, 1970; González-Ferrán *et al.*, 1971; Robool, 1973; Baker *et al.*, 1975; Robool, 1979; Weaver *et al.*, 1979; Tarney *et al.*, 1982; Keller *et al.*, 1992; Smellie *et al.*, 1992; De Rosa *et al.*, 1995; Fretzdorff and Smellie, 2002; Smellie *et al.*, 2002). However, most of these data are major element analyses, while trace and rare earth element data are scarce. Moreover, only one paper includes also major element analyses from bulk tephra sampled at the source volcano (Valenzuela *et al.*, 1970), though not from tephra glass.

The data record for the other volcanic centers around the northern Antarctic Peninsula exhibits substantial gaps, and detailed tephra studies have so far been undertaken at none of them. The demand for such data is also reflected by numerous studies of ice cores, lake and marine sediment cores in the Antarctic Peninsula - South Shetland Islands - Southern Oceans area that quote the volcanic source of the recognized tephra layers as 'unknown' (*e.g.*, Fretzdorff and Smellie, 2002). The missing chemical and age data from tephra (particularly trace and REE compositions and the major element volcanic glass compositions) so far largely precluded a possible attribution of layers of unknown origin to specific subaerial Antarctic Peninsula volcanoes. However,

some tephra layers found in marine sediment cores might also originate from submarine volcanoes in the Bransfield and Larsen rifts, which are not covered by this study.

9. Implications for regional climate systems

One scope of our work was to support future studies on local (*i.e.*, Antarctic Peninsula) climatic events and patterns in past and present as displayed by the tephra dispersal, super-regional air mass trajectories (particularly towards the Antarctic main continent) and the eventual impact of the volcanic eruptions on local climate.

The impact of Antarctic Peninsula volcanism on the climate of the Southern Hemisphere is less understood than the better studied and modeled impact of volcanic eruptions on Northern Hemisphere climate (*e.g.*, Robock, 1978, 1981; Stothers and Rampino, 1983; Crowley *et al.*, 1993; Ammann *et al.*, 2003; Oman *et al.*, 2006; Timmreck and Graf, 2006; Fischer *et al.*, 2007). Reconstructions developed from historical data (Andronova *et al.*, 1999; Crowley and Kim, 1999) and multiple ice core records (Robock and Free, 1995; Ammann *et al.*, 2003; Gao *et al.*, 2008) do not use any Antarctic Peninsula volcanic eruptions for their climate forcing time series. Only a single climate impact simulation of the tropical 1991 Mount Pinatubo eruption on the Southern Hemisphere (Robock *et al.*, 2007) is available.

The potential impact of the Antarctic Peninsula volcanoes on regional climate is related to seasonality, magnitude and duration of the volcanic eruptions. The seasonality of an eruption can impact the formation and preservation of sea ice in the region, both of which are shown to be major factors controlling seasonal temperatures, especially during the winter months. The distribution of the volcanic products around the continent is influenced by the intensity of the polar vortex and the height of the tropopause. However, among the studied volcanoes, Deception Island is probably the only candidate capable of generating an eruption that is sufficiently strong (subplinian to plinian) to impact even distant parts of the Antarctic continent.

Once information on the magnitudes and timing of Antarctic volcanism will become available, we should expect to find potential climate related events in paleoclimate records (*e.g.*, ice cores and lake sediment cores collected in the region). Modern day data from satellite sensors and direct climate observations provide only limited help to decipher information on climate forcing from regional volcanoes because only small volcanic eruptions were observed during the last forty years (*e.g.*, the Deception Island eruptions in 1967-1970 compared to the same volcano's pre-historical activity as summarized by Martí and Baraldo (1990) and Smellie (2001)). Increased anthropogenic emissions further complicate the detection of volcanic products in ice core sulphate records covering modern time intervals, and the evaluation of the impact of such events, by masking the volcanic signal. To obtain this information, combined long term paleoclimate and volcanic time series have to be developed in order to determine the impact of Antarctic volcanic eruptions.

Antarctic ice cores allow quantitative estimates of fluxes of volcanically derived aerosols like SO_4^{2-} to the atmosphere. Unfortunately, the sulphate increase in ice cores only yields information on the timing of the potential source eruption, but not the chemical signature.

Tephra has one pronounced advantage over sulphate spikes: besides the timing of the respective eruption it also reveals the chemical fingerprint of the erupted material and thus allows identifying the source volcano. Once the source volcano of a given tephra layer is known, additional information on climatic conditions at the time of eruption (*e.g.*, atmospheric circulation patterns controlling air mass trajectories, wind direction) can be deduced.

10. Summary and Conclusions

The developed dataset (http://dx.doi.org/10.1594/IEDA/100052) contributes to establishing a regional tephrochronological framework that includes information on Late Pleistocene-Holocene volcanic centers located in the northern part of the Antarctic Peninsula along two active rift systems (Larsen Rift and Bransfield Rift).

The vast majority of the regional volcanic products are basalts and basaltic andesites. The exceptions are Paulet Island, which is entirely of trachybasaltic composition, and some of the samples from Deception Island, which are basaltic trachyandesites and rarely even trachydacites.

The Larsen Rift volcanoes, as a general rule, feature SiO_2<53 wt%. The Cape Purvis volcano and

Paulet Island have K_2O-values higher than 1 wt%, a condition that is only partly met by the samples from the Seal Nunataks. Except for the most evolved samples, the Bransfield Strait volcanoes feature K_2O-contents well below 1 wt%.

Crustal contamination during differentiation in shallow level magma chambers has not occurred or was insignificant, as indicated, *e.g.*, by Sr-Nd-Pb isotope systematics.

Microprobe analyses on the glass component reveal fundamental differences between eastern and western Antarctic Peninsula volcanoes. As a general rule, the glass component of the Bransfield Rift volcanoes shows moderately to strongly elevated SiO_2 but not or only slightly elevated alkali-contents as compared to the respective bulk rock composition. In contrast, the glass component of the Larsen Rift volcanoes is only slightly enriched in SiO_2 but moderately to strongly in alkalis. We interpret this to reflect differences in the geotectonic setting, Larsen Rift representing an intra-plate environment, while Bransfield Rift is a marginal basin with back-arc-like characteristics, situated behind an inactive magmatic arc.

In order to identify the source of distal tephra layers of unknown origin, a step-by-step strategy resembling a flow chart has been developed. Application of this 'Decision Tree' is based on the successive exclusion of potential source volcanoes until zooming in on the last remaining candidate, which is the most likely source for the tephra layer in question in case the unknown tephra fulfils the geochemical conditions (Fig. 16).

Nb/Y ratios higher than 0.67 in combination with low Sr/Nb ratios and strongly enriched LREE (expressed, *e.g.*, as very low Ba/La) seem to be diagnostic to distinguish the volcanoes located along the Larsen Rift (Cape Purvis volcano, Paulet Island and Seal Nunataks) from those associated with Bransfield Rift (Sail Rock, Deception Island, Rezen Peak, Inott Point, Penguin Island, Melville Peak and Bridgeman Island).

Sr-contents and Sr/Y ratio proved useful to distinguish between the different volcanoes of the Larsen Rift group. To separate the Bransfield Rift volcanoes from each other, Nb/Y, Th/Nb, Th/Yb, and LREE patterns along with Ba/Th and Sr/Y appear to be diagnostic and powerful tools.

The application of the step-by-step approach on ice tephras from central Livingston Island confirmed previously published work in showing that all ice tephras unequivocally originated from the Deception Island volcano, situated some 40 km southwest of central Livingston Island.

The correlation of our new data with published data from tephra layers identified in ice, lake and marine sediment cores, as well as with new data obtained from the CASA project (Climate of the Antarctic and South America (CASA): Joint Brazilian-Chilean-US ice core drilling on the Detroit Plateau, Antarctic Peninsula) will contribute substantially to a better understanding and interpretation of individual climatic events as well as tendencies in the climatic evolution of the northern Antarctic Peninsula, maybe also within a superregional frame (Antarctic continent, Southern Oceans). The data set will contribute also to the development of a new Antarctic tephrochronological framework. The ability to reliably identify the eruption(s) responsible for a particular signal provides the information needed to clearly assess the climatic forcing capability of a particular eruption/volcano and of a particular type of eruption.

Acknowledgements

This project was funded by the Instituto Antártico Chileno (INACH, project number OA_05-07) and by the NOAA (Department of Commerce grant: NA08OAR4310867). The Chilean Navy and the Brazilian, Bulgarian, Korean and Spanish Antarctic Programs substantially supported fieldwork and logistics.

The Antarctic stations of Bulgaria, Chile and Spain served as bases for fieldwork on Livingston, King George, and Deception Island, respectively. J. Smellie and R. Keller are gratefully acknowledged for their positive, constructive reviews and thoughtful comments. E. Domack kindly provided a sample he collected in February 2010 close to the Argentine Base Matienzo at Larsen Nunatak (Seal Nunataks). Furthermore, we thank the Climate Change Institute and Department of Earth Sciences (both University of Maine) for substantial logistic and laboratory support.

References

Alloway, B.V.; Lowe, D.J.; Barrell, D.J.A.; Newnham, R.M.; Almond, P.C.; Augustinus, P.C.; Bertler, N.A.N.; Carter, L.; Litchfield, N.J.; McGlone, M.S.; Shulmeister, J.; Vandergoes, M.J.; Williams, P.W.; NZ-INTIMATE members 2007. Towards a climate event stratigraphy for New Zealand over the past

30,000 years (NZ-INTIMATE project). Journal of Quaternary Science 22: 9-35.

Ammann, C.; Meehl, G.; Washington, W.; Zender, C. 2003. A monthly and latitudinally varying volcanic forcing dataset in simulations of the 20th century climate. Geophysical Research Letters 30 (12): p. 1657.

Andronova, N.; Rozanov, E.; Yang, F.; Schlesinger, M.; Stenchikov, G. 1999. Radiative forcing by volcanic aerosols from 1850 to 1994. Journal of Geophysical Research 104 (D14): 16807-16826.

Aristarain, A.J.; Delmas, R.J. 1998. Ice record of a large eruption of Deception Island Volcano (Antarctica) in the XVIIth century. Journal of Volcanology and Geothermal Research 80: 17-25.

Aristarain, A.J.; Jouzel, J.; Lorius, C. 1990. A 400 years isotope record of the Antarctic Peninsula climate. Geophysical Research Letters 17: 2369-2372.

Ashcroft, W.A. 1972. Crustal structure of the South Shetland Islands and the Bransfield Strait. British Antarctic Survey Scientific Reports 66: 43 p.

Baker, P.E.; McReath, I.; Harvey, M.R.; Roobol, M.J.; Davies, T.G. 1975. The geology of the South Shetland Islands: V. Volcanic evolution of Deception Island. British Antarctic Survey Scientific Reports 78: 81 p.

Baker, P.E.; Buckley, F.; Rex, D.C. 1977. Cenozoic volcanism in the Antarctic. Philosophical Transactions of the Royal Society of London B279: 131-142.

Baraldo, A.; Rinaldi, C.A. 2000. Stratigraphy and structure of Deception Island, South Shetland Islands, Antarctica. Journal of South American Earth Sciences 13: 785-769.

Barker, P.F. 1976. The tectonic framework of Cenozoic volcanism in the Scotia Sea region–A review. *In* Proceedings of the Symposium on Andean and Antarctic Volcanology Problems (González-Ferrán, O.; editor). International Association of Volcanology and Chemistry of the Earth's Interior: 330-346. Rome.

Barker, P.F. 1982. The Cenozoic subduction history of the Pacific margin of the Antarctic Peninsula: ridge-crest trench interactions. Journal of the Geological Society of London 139: 787-801.

Barker, P.F.; Dalziel, I.W.D.; Storey, B.C. 1991. Tectonic development of the Scotia arc region. *In* The geology of Antarctica (Tingey, R.J.: editor). Oxford Science Publ., Monograph on Geology and Geophysics 17, Clarendon Press: 215-248.

Barton, C.M. 1965. The geology of the South Shetland Islands: III. The stratigraphy of King George Island. British Antarctic Survey Scientific Reports 44: 33 p.

Basile, I.; Petit, J.R.; Touron, S.; Grousset, F.E.; Barkov, N. 2001. Volcanic layers in Antarctic (Vostok) ice cores: Source identification and atmospheric implications. Journal of Geophysical Research 106 (D23): 31915-31931.

Ben-Zvi, T.; Wilcock, W.S.D.; Barclay, A.H.; Zandomeneghi, D.; Ibáñez, J.M.; Almendros, J. 2007. The P-Wave velocity structure of Deception Island, Antarctica, from two-dimensional seismic tomography. *In* Antarctica: A Keystone in a Changing World - Online Proceedings of the 10th ISAES (Cooper, A.K.; Raymond, C.K.; editors). U.S. Geological Survey (USGS) Open-File Report 2007-1047, Extended Abstract 078: 5 p.

Ben-Zvi, T.; Wilcock, W.S.D.; Barclay, A.H.; Zandomeneghi, D.; Ibáñez, J.M.; Almendros, J. 2009. The P-wave velocity structure of Deception Island, Antarctica, from two-dimensional seismic tomography. Journal of Volcanology and Geothermal Research 180: 67-80.

Birkenmajer, K. 1980. Age of the Penguin Island volcano, South Shetland Islands (West Antarctica), by the Lichenometric method. Bulletin de la Academie Polonaise des Sciences - Serie des Sciences de la Terre 27: 69-76.

Birkenmajer, K. 1994. Evolution of the Pacific margin of the northern Antarctic Peninsula: an overview. Geologische Rundschau 83: 309-321.

Birkenmajer, K. 2001. Mesozoic and Cenozoic stratigraphic units in parts of the South Shetland Islands and northern Antarctic Peninsula (as used by the Polish Antarctic Programmes). Studia Geologica Polonica 118: 188 p.

Birkenmajer, K.; Keller, R.A. 1990. Pleistocene age of the Melville Peak volcano, King George Island, West Antarctica, by K-Ar dating. Bulletin of the Polish Academy of Sciences, Earth Sciences 38: 17-24.

Birkenmajer, K.; Delitala, M.C.; Narebski, W.; Nicoletti, M.; Petrucciani, C. 1986a. Geochronology of Tertiary island-arc volcanics and glacigenic deposits, King George Island, South Shetland Islands (West Antarctica). Bulletin de la Academie Polonaise des Sciences - Serie des Sciences de la Terre 34: 257- 273.

Birkenmajer, K.; Kaiser, G.; Narebski, W.; Pilot, J.; Rösler, H.J. 1986b. Age of magmatic complexes of the Barton Horst, King George Island (South Shetland Islands, West Antarctica), by K-Ar dating. Bulletin of the Polish Academy of Sciences, Earth Sciences 34: 139-155.

Birkenmajer, K.; Guterch, A.; Grad, M.; Janik, T.; Perchuc, E. 1990. Lithospheric transect Antarctic Peninsula-South Shetland Islands, Antarctica. Polish Polar Research 11: 241-258.

Birkenmajer, K.; Francalanci, L.; Peccerillo, A. 1991. Petrological and geochemical constraints on the genesis of Mesozoic-Cenozoic magmatism of King

George Island, South Shetland Islands, Antarctica. Antarctic Science 3: 293-308.

Björck, S.; Sandgren, P.; Zale, R. 1991a. Late Holocene tephrochronology of the northern Antarctic Peninsula. Quaternary Research 36: 322-328.

Björck, S.; Håkansson, H.; Zale, R.; Karlén, W.; Liedberg Jönsson, B. 1991b. A late Holocene lake sediment sequence from Livingston Island, South Shetland Islands, with palaeoclimatic implications. Antarctic Science 3: 61-72.

Björck, S.; Malmer, N.; Hjort, C.; Sandgren, P.; Ingólfsson, Ò.; Wallén, B.; Lewis Smith, R.I.; Liedberg Jönsson, B.L. 1991c. Stratigraphic and paleoclimatic studies of a 5,500-year-old moss bank on Elephant Island, Antarctica. Arctic and Alpine Research 23: 361-374.

Björck, S.; Håkansson, H.; Olsson, S.; Barnekow, L.; Janssens, J. 1993. Palaeoclimatic studies in the South Shetland Islands, Antarctica, based on numerous stratigraphic variables in lake sediments. Journal of Paleolimnology 8: 233-272.

Budner, D.; Cole-Dai, J. 2003. The Number and Magnitude of Large Explosive Volcanic Eruptions Between 904 and 1865 A.D.: Quantitative Evidence From a New South Pole Ice Core. *In* Volcanism and the Earth's Atmosphere, AGU Geophysical Monograph 139: 165-176. doi: 10.1029/139GM10.

Cole-Dai, J.; Moseley-Thompson, E.; Wight, S.P.; Thompson, L.G. 2000. A 4100-year record of explosive volcanism from an East Antarctic ice core. Journal of Geophysical Research 105 (D19): 24431-24441.

Coulter, S.E.; Pilcher, J.R.; Hall, V.A.; Plunkett, G.; Davies, S.M. 2010. Testing the reliability of the JEOL FEGSEM 6500F electron microprobe for quantitative major element analysis of glass shards from rhyolitic tephra. Boreas 39: 163-169. doi: 10.1111/j.1502-3885.2009.00113.x. ISSN 0300-9483.

Crowley, T.J.; Kim, K.-Y. 1999. Modeling the temperature response to forced climate change over the past six centuries. Geophysical Research Letters 26: 1901-1904.

Crowley, T.J.; Criste, T.A.; Smith, N. 1993. Reassessment of Crete (Greenland) ice core acidity/volcanism link to climate change. Geophysical Research Letters 20 (3): 209-212.

Davey, F.J. 1972. Marine gravity measurements in Bransfield Strait and adjacent areas. *In* Antarctic geology and geophysics (Adie, R.J.; editor). Universitetsforlaget: 39-46. Oslo.

De Angelis, M.; Fehrenbach, L.; Jéhanno, C.; Maurette, M. 1985. Micrometre-sized volcanic glasses in polar ice and snows. Nature 317: 52-54.

De Rosa, R.; Mazzuoli, R.; Omarini, R.H.; Ventura, G.; Viramonte, J.G. 1995. A Volcanological Model for the Historical Eruptions at Deception Island (Bransfield Strait, Antarctica). Terra Antartica 2 (2): 95-101.

Delmas, R.J.; Kirchner, S.; Palais, J.M.; Petit, J.-R. 1992. 1000 years of explosive volcanism recorded at the South Pole. Tellus 44(B): 335-350.

Dietrich, R.; Dach, R.; Engelhardt, G.; Ihde, J.; Korth, W.; Kutterer, H.; Lindner, K.; Mayer, M.; Menge, F.; Miller, H.; Müller, C.; Niemeier, W.; Perlt, J.; Pohl, M.; Salbach, H.; Schenke, H.-W.; Schöne, T.; Seeber, G.; Veit, A.; Völksen, C. 2000. Ergebnisse der SCAR GPS Kampagnen-ITRF-Koordinaten und Geschwindigkeiten. *In* Deutsche Beiträge zu GPS-Kampagnen des Scientific Committee on Antarctic Research (SCAR) (Dietrich, R.; editor), 1995-1998, Reihe B, Angewandte Geodäsie 310: 11-20.

Dunbar, N.W.; Kurbatov, A.V. 2011: Tephrochronology of the Siple Dome ice core, West Antarctica: correlations and sources. Quaternary Science Reviews 30 (13-14): 1602-1614.

Dunbar, N.W.; Zielinski, G.A.; Voisin, D.T. 2003. Tephra layers in the Siple Dome and Taylor Dome Ice Cores, Antarctica: Sources and correlations. Journal of Geophysical Research 108 (B8): 2374. doi: 10.1029/2002JB002056.

Elliott, T. 2003. Tracers of the slab. *In* Inside the subduction factory (Eiler, J.; editor). AGU Geophysical Monographs 138: 23-45.

Fischer, E.; Luterbacher, J.; Zorita, E.; Tett, S.F.B.; Casty, C.; Wanner, H. 2007. European climate response to tropical volcanic eruptions over the last half millennium. Geophysical Research Letters 34 (5): L05707.

Fretzdorff, S.; Smellie, J.L. 2002. Electron microprobe characterization of ash layers in sediments from the central Bransfield basin (Antarctic Peninsula): evidence for at least two volcanic sources. Antarctic Science 14 (4): 412-421.

Fretzdorff, S.; Worthington, T.J.; Haase, K.M.; Hékinian, R.; Franz, L.; Keller, R.A.; Stoffers, P. 2004. Magmatism in the Bransfield Basin: Rifting of the South Shetland Arc? Journal of Geophysical Research 109, B12208. doi: 10.1029/2004JB003046.

Fujii, Y.; Kohno, M.; Motoyama, H.; Matoba, S.; Watanabe, O.; Fujita, S.; Azuma, N.; Kikuchi, T.; Fukuoka, T.; Suzuki, T. 1999. Tephra layers in the Dome Fuji (Antarctica) deep ice core. Annals of Glaciology 29 (1): 126-130.

Gao, C.; Robock, A.; Ammann, C. 2008. Volcanic forcing of climate over the past 1500 years: An improved ice core-based index for climate models. Journal of Geophysical Research 113, D23111. doi: 10.1029/2008JD010239.

Gibson, J.A.E.; Zale, R. 2006. Holocene development of the fauna of Lake Boeckella, northern Antarctic Peninsula. The Holocene 16 (5): 625-634.

González-Casado, J.M.; Giner-Robles, J.L.; López-Martínez, J. 2000. Bransfield Basin, Antarctic Peninsula: Not a normal backarc basin. Geology 28 (11): 1043-1046.

González-Ferrán, O. 1983. The Larsen Rift: an active extension fracture in West Antarctica. *In* Antarctic Earth Science (Oliver, R.; James, P.; Jago, J.; editors). Cambridge University Press, Melbourne: 344-346.

González-Ferrán, O. 1995. Volcanes de Chile. Instituto Geográfico Militar: 635 p. Santiago, Chile.

González-Ferrán, O.; Katsui, Y. 1970. Estudio integral del volcanismo cenozoico superior de las Islas Shetland del Sur, Antártida. Serie Científica del Instituto Antártico Chileno 1, No. 2: 123-174.

González-Ferrán, O.; Munizaga, F.; Moreno, H. 1971. 1970 eruption at Deception Island: distribution and chemical features of ejected materials. Antarctic Journal of the United States, July-August 1971: 87-89.

Griffiths, D.H.; Riddihough, R.P.; Cameron, H.A.D.; Kennett, P. 1964. Geological investigation of the Scotia Arc. British Antarctic Survey Scientific Reports 46: 43 p.

Han, J.; Xie, Z.; Dai, F.; Zhang, W. 1999. Volcanic eruptions recorded in an ice core from Collins Cap, King George Island, Antarctica. Annals of Glaciology 29: 121-125.

Harpel, C.J.; Kyle, P.R.; Dunbar, N.W. 2008. Englacial tephrostratigraphy of Erebus volcano, Antarctica. Journal of Volcanology and Geothermal Research 177 (3): 549-568.

Hawkes, D.D. 1961. The geology of the South Shetland Islands: II. The geology and petrology of Deception Island. Falkland Islands Dependencies Survey Scientific Reports 27: 43 p.

Hawkesworth, C.; Turner, S.; Peate, D.; McDermott, F.; van Calsteren, P. 1997. Elemental U and Th variations in island arc rocks: implications for U-series isotopes. Chemical Geology 139: 207-221.

Henriet, J.P.; Meissner, R.; Miller, H.; GRAPE Team. 1992. Active margin processes along the Antarctic Peninsula. Tectonophysics 201: 229-253.

Hildreth, W.; Halliday, A.N.; Christiansen, R.L. 1991. Isotopic and chemical evidence concerning the genesis and contamination of basaltic and rhyolitic magma beneath the Yellowstone Plateau Volcanic Field. Journal of Petrology 32 (1): 63-138.

Hillenbrand, C.-D.; Moreton, S.G.; Caburlotto, A.; Pudsey, C.J.; Lucchi, R.G.; Smellie, J.L.; Benetti, S.; Grobe, H.; Hunt, J.B.; Larter, R.D. 2008. Volcanic time-markers for Marine Isotopic Stages 6 and 5 in Southern Ocean sediments and Antarctic ice cores: implications for tephra correlations between palaeoclimatic records. Quaternary Science Reviews 27 (5-6): 518-540.

Hodgson, D.A.; Dyson, C.L.; Jones, V.J.; Smellie, J.L. 1998. Tephra analysis of sediments from Midge Lake (South Shetland Islands) and Sombre Lake (South Orkney Islands), Antarctica. Antarctic Science 10 (1): 13-20.

Hofmann, A.W.; Jochum, K.P.; Seufert, M.; White, W.M. 1986. Nb and Pb in oceanic basalts: new constraints on mantle evolution. Earth and Planetary Science Letters 79: 33-45.

Hole, M.J. 1990. Geochemical evolution of Pliocene-Recent postsubduction alkalic basalts from Seal Nunataks, Antarctic Peninsula. Journal of Volcanology and Geothermal Research 40: 149-167.

Hole, M.J.; Kempton, P.D.; Millar, I.L. 1993. Trace element and isotope characteristics of small-degree melts of the asthenosphere; evidence from the alkalic basalts of the Antarctic Peninsula. Chemical Geology 109: 51-68.

Hubberten, H.-W.; Morche, W.; Westall, F.; Fütterer, D.K.; Keller, J. 1991. Geochemical investigations of volcanic ash layers from southern Atlantic Legs 113 and 114. Proceedings of the Ocean Drilling Project, Scientific Results 114: 733-749.

Ibáñez, J.M.; Almendros, J.; Carmona, E.; Martínez-Arévalo, C.; Abril, M. 2003. The recent seismo-volcanic activity at Deception Island volcano. Deep-Sea Research II 50: 1611-1629.

Jordan, T.A.; Ferraccioli, F.; Jones, P.C.; Smellie, J.L.; Ghidella, M.; Corr, H.; Zakrajsek, A.F. 2007. High-resolution airborne gravity imaging over James Ross Island (West Antarctica). *In* Antarctica: A Keystone in a Changing World - Online Proceedings of the 10th ISAES (Cooper, A.K.; Raymond, C.K.; editors), U.S. Geological Survey (USGS) Open-File Report 2007-1047, Short Research Paper 060: 4 p.

Karlof, L.; Winther, J.-G.; Isaksson, E.; Kohler, J.; Pinglot, J.F.; Wilhelms, F.; Hansson, M.; Holmlund, P.; Nyman, M.; Pettersson, R.; Stenberg, M.; Thomassen, M.P.A.; van der Veen, C.; van der Walt, R.S.W. 2000. A 1500 year record of accumulation at Amundsenisen western Dronning Maud Land, Antarctica, derived from electrical and radioactive measurements on a

120 m ice core. Journal of Geophysical Research 105 (D10): 12471-12483.

Keller, R.A.; Fisk, M.R.; White, W.M.; Birkenmajer, K. 1992. Isotopic and trace element constraints on mixing and melting models of marginal basin volcanism, Bransfield Strait, Antarctica. Earth and Planetary Science Letters 111: 287-303.

Keller, R.A.; Fisk, M.R.; Smellie, J.L.; Strelin, J.A.; Lawver, L.A.; White, W.M. 2002. Geochemistry of back arc basin volcanism in Bransfield Strait, Antarctica: Subducted contributions and along-axis variations. Journal of Geophysical Research 107 (B8). doi: 10.1029/2001JB000444.

Keller, R.A.; Domack, E.; Drake, A. 2003. Potential for tephrochronology of marine sediment cores from Bransfield Strait and the northwestern Weddell Sea. *In* 16th INQUA Congress, Geological Society of America, Abstracts with Programs: p. 236. Reno, U.S.A.

Košler, J.; Magna, T.; Mlčoch, B.; Mixa, P.; Nývlt, D.; Holub, F.V. 2009. Combined Sr, Nd, Pb and Li isotope geochemistry of alkaline lavas from northern James Ross Island (Antarctica Peninsula) and implications for back-arc magma formation. Chemical Geology 258: 207-218.

Kraus, S. 2005. Magmatic dyke systems of the South Shetland Islands volcanic arc (West Antarctica): reflections of the geodynamic history. Dissertation, Ludwig-Maximilians-University Munich, Faculty of Geosciences: 160 p. http://nbn-resolving.de/urn:nbn:de:bvb:19-38277.

Kraus, S.; Kurbatov, A. 2010. Chapter 5: Chemical fingerprint of bulk tephra from Late Pleistocene / Holocene volcanoes in the northern Antarctic Peninsula area. *In* Antarctica: Global, Environmental and Economic Issues (Mulder, T.J.; editor). Nova Publishers, New York: 193-215. https://www.novapublishers.com/catalog/product_info.php?products_id=18211.

Kraus, S.; Miller, H.; Dimov, D.; Hegner, E.; McWilliams, M.; Pecscay, Z. 2008. Structural geology of the Miers Bluff Formation (Upper Jurassic-Upper Cretaceous) and crosscutting Paleogene dikes (Livingston Island, South Shetland Islands, Antarctica) - insights into the geodynamic history of the northern Antarctic Peninsula. Journal of South American Earth Sciences 26 (4): 498-512.

Kraus, S.; Poblete, F.; Arriagada, C. 2010. Dike systems and their volcanic host rocks on King George Island, Antarctica: Implications on the geodynamic history based on a multidisciplinary approach. Tectonophysics 495 (3-4): 269-297.

Kurbatov, A.V.; Zielinski, G.A.; Dunbar, N.W.; Mayewski, P.A.; Meyerson, E.A.; Sneed, S.B.; Taylor, K.C. 2006. A 12,000 year record of explosive volcanism in the Siple Dome Ice Core, West Antarctica. Journal of Geophysical Research 111, D12307. doi: 10.1029/2005JD006072.

Kyle, P.R.; Jezek, P.A.; Mosley-Thompson, E.; Thompson, L.G. 1981. Tephra layers in the Byrd Station ice core and the Dome C ice core, Antarctica, and their climatic importance. Journal of Volcanology and Geothermal Research 11 (1): 29-39.

Lane, C.S.; Andrič, M.; Cullen, V.L.; Blockley, P.E. 2011. The occurrence of distal Icelandic and Italian tephra in the Lateglacial of Lake Bled, Slovenia. Quaternary Science Reviews 30 (9-10): 1013-1018.

Lane, C.S.; De Klerk, P.; Cullen, V.L. 2012. A tephrochronology for the Lateglacial palynological record of the Endinger Bruch (Vorpommern, north-eastern Germany). Journal of Quaternary Science 27 (2): 141-149.

Larsen, C.A. 1894. The voyage of the Jason to the Antarctic regions. Geographical Journal 4: 333-344.

Larter, R.D.; Barker, P.F. 1991. Effects of ridge-crest trench interaction on Antarctic-Phoenix Spreading: Forces on a young subducting plate. Journal of Geophysical Research 96: 19583-19607.

Lawver, L.A.; Keller, R.A.; Fisk, M.R.; Strelin, J.A. 1995. Bransfield Strait, Antarctic Peninsula: Active extension behind a dead arc. *In* Back-arc basins: Tectonics and magmatism (Taylor, B.; editor). Plenum Press, Amsterdam: 315-342.

Le Maitre, R.W. 2002. Igneous rocks: a classification and glossary of terms. Recommendations of the International Union of Geological Sciences subcommission on the systematics of igneous rocks. Cambridge University Press: 252 p.

LeMasurier, W.E.; Thomson, J.W. 1990. Volcanoes of the Antarctic Plate and Southern Oceans. AGU Antarctic Research Series 48: 487 p.

Lowe, D.J. 2008. Globalization of tephrochronology: new views from Australasia. Geography 32 (3): 311-335.

Lowe, D.J. 2011. Tephrochronology and its application: A review. Quaternary Geochronology 6: 107-153.

Machado, A.; Chemale, F.; Conceição, R.V.; Kawaskita, K.; Morata, D.; Oteíza, O.; Van Schmus, W.R. 2005. Modeling of subduction components in the genesis of the Meso-Cenozoic igneous rocks from the South Shetland Arc, Antarctica. Lithos 82 (3): 435-453.

Maestro, A.; Somoza, L.; Rey, J.; Martínez-Frías, J.; López-Martínez, J. 2007. Active tectonics, fault patterns, and stress field of Deception Island: A response

to oblique convergence between the Pacific and Antarctic plates. Journal of South American Earth Sciences 23: 256-268.

Martí, A.; Baraldo, A. 1990. Pre-caldera pyroclastic deposits of Deception Island (South Shetland Islands). Antarctic Science 2: 345-352. doi:10.1017/S0954102090000475.

Martí, J.; Vila, J.; Rey, J. 1996. Deception Island (Bransfield Strait, Antarctica): an example of a volcanic caldera developed by extensional tectonics. *In* Volcano instability on the earth and other planets (McGuire, W.J.; Jones, A.P.; Neuberg, J.; editors). Geological Society of London Special Publication 110: 253-265.

Matthies, D.; Storzer, D.; Troll, G. 1988. Volcanic ashes in Bransfield Strait sediments: geochemical and stratigraphical investigations (Antarctica). Proceedings of the Second International Conference on Natural Glasses, Prague: 139-147.

Merlet, C. 1994. An accurate computer correction program for quantitative electron probe microanalysis. Mikrochimica Acta 114/115: 363-376.

Millar, I.L.; Willan, R.C.R.; Wareham, C.D.; Boyce, A.J. 2001. The role of crustal and mantle sources in the genesis of granitoids of the Antarctic Peninsula and adjacent crustal blocks. Journal of the Geological Society of London 158: 885-867.

Miller, D.M.; Goldstein, S.L.; Langmuir, C.H. 1994. Cerium/lead and lead isotope ratios in arc magmas and the enrichment of lead in the continents. Nature 368: 514-520.

Moreton, S.; Smellie, J.L. 1998. Identification and correlation of distal tephra layers in deep-sea sediment cores, Scotia Sea, Antarctica. Annals of Glaciology 27: 285-289.

Muñoz-Martín, A.; Catalán, M.; Martín-Dávila, J.; Carbo, A. 2005. Upper crustal structure of Deception Island area (Bransfield Strait, Antarctica) from gravity and magnetic modeling. Antarctic Science 17 (2): 213-224.

Narcisi, B.; Proposito, M.; Frezzotti, M. 2001. Ice record of a 13th century explosive volcanic eruption in northern Victoria Land, East Antarctica. Antarctic Science 13 (2): 174-181.

Narcisi, B.; Petit, J.R.; Delmonte, B.; Basile-Doelsch, I.; Maggi, V. 2005. Characteristics and sources of tephra layers in the EPICA-Dome C ice record (East Antarctica): Implications for past atmospheric circulation and ice core stratigraphic correlations. Earth and Planetary Science Letters 239 (3-4): 253-265.

Narcisi, B.; Petit, J.R.; Tiepolo, M. 2006. A volcanic marker (92 ka) for dating deep east Antarctic ice cores. Quaternary Science Reviews 25 (21-22): 2682-2687.

Narcisi, B.; Petit, J.R.; Chappellaz, J. 2010a. A 70 ka record of explosive eruptions from the TALDICE ice core (Talos Dome, East Antarctic plateau). Journal of Quaternary Science 25 (6): 844-849.

Narcisi, B.; Petit, J.R.; Delmonte, B. 2010b. Extended East Antarctic ice-core tephrostratigraphy. Quaternary Science Reviews 29 (1-2): 21-27.

Newton, A.J.; Dugmore, A.J.; Gittings, B.M. 2007. Tephrabase: tephrochronology and the development of a centralized European database. Journal of Quaternary Science 22 (7): 737-743.

Oman, L.; Robock, A.; Stenchikov, G.L.; Thordarson, T. 2006. High-latitude eruptions cast shadow over the African monsoon and the flow of the Nile. Geophysical Research Letters 33, L18711. doi:10.1029/2006GL027665.

Palais, J.M.; Kyle, P.R. 1988. Chemical composition of ice containing tephra layers in the Byrd Station ice core, Antarctica. Quaternary Research 30 (3): 315-330.

Palais, J.M.; Kirchner, S.; Delmas, R. 1989. Identification and correlation of volcanic eruption horizons in a 1,000-year ice core record from the South Pole. Antarctic Journal of the United States 24: 101-104.

Palais, J.M.; Germani, M.S.; Zielinski, G.A. 1992. Interhemispheric transport of volcanic ash from a 1259 A.D. volcanic eruption to the Greenland and Antarctic ice sheets. Geophysical Research Letters 19 (8): 801-804.

Pallás, R.; Smellie, J.L.; Casas, J.M.; Calvet, J. 2001. Using tephrochronology to date temperate ice: correlation between ice tephras on Livingston Island and eruptive units on Deception Island volcano (South Shetland Islands, Antarctica). Holocene 11 (2): 149-160.

Pankhurst, R.J.; Smellie, J.L. 1983. K-Ar geochronology of the South Shetland Islands, lesser Antarctica: Apparent lateral migration of Jurassic to Quaternary island arc volcanism. Earth and Planetary Science Letters 66: 214-222.

Pearce, J.A.; Leat, P.T.; Barker, P.F.; Millar, I.L. 2001. Geochemical tracing of Pacific-to-Atlantic upper-mantle flow through the Drake Passage. Nature 410: 457-461.

Pearce, N.J.G.; Denton, J.S.; Perkins, W.T.; Westgate, J.A.; Alloway, B.V. 2007. Correlation and characterization of individual glass shards from tephra deposits using trace element laser ablation ICP-MS analyses: current status and future potential. Journal of Quaternary Science 22: 721-736.

Pérez-López, R.; Giner-Robles, J.L.; Martínez-Díaz, J.J.; Rodríguez-Pascua, M.A.; Bejar, M.; Paredes, C.; González-Casado, J.M. 2007. Active tectonics on

Deception Island (West-Antarctica): A new approach by using the fractal anisotropy of lineaments, fault slip measurements and the caldera collapse shape. *In* Antarctica: A Keystone in a Changing World - Online Proceedings of the 10th ISAES (Cooper, A.K.; Raymond, C.R.; editors), U.S. Geological Survey (USGS) Open-File Report 2007-1047, Short Research Paper 086: 4 p.

Rex, D.C. 1976. Geochronology in relation to stratigraphy of the Antarctic Peninsula. British Antarctic Survey Bulletin 43: 49-58.

Rey, J.; Somoza, L.; Martínez-Frías, J. 1995. Tectonic, volcanic, and hydrothermal event sequence on Deception Island (Antarctica). Geo-Marine Letters 15: 1-8.

Robertson Maurice, S.D.; Wiens, D.A.; Shore, P.J.; Smith, G.P.; Vera, E. 2002. Seismicity and tectonics of the South Shetland Islands and Bransfield Strait from the SEPA broadband seismograph deployment. Royal Society of New Zealand Bulletin 35: 549-554.

Robertson Maurice, S.D.; Wiens, D.A.; Shore, P.J.; Vera, E.; Dorman, L.M. 2003. Seismicity and tectonics of the South Shetland Islands and Bransfield Strait from a regional broadband seismograph deployment. Journal of Geophysical Research 108 (B10): 2461-2473.

Robock, A. 1978. Internally and externally caused climate change. Journal of Atmospheric Sciences 35: 1111-1122.

Robock, A. 1981. A latitudinally dependent volcanic dust veil index, and its effect on climate simulations. Journal of Volcanology and Geothermal Research 11: 67-80.

Robock, A.; Free, M. 1995. Ice cores as an index of global volcanism from 1850 to the present. Journal of Geophysical Research 100 (D6): 11549-11568.

Robock, A.; Adams, T.; Moore, M.; Oman, L.; Stenchikov, G. 2007. Southern Hemisphere atmospheric circulation effects of the 1991 Mount Pinatubo eruption. Geophysical Research Letters 34, L23710. doi:10.1029/2007GL031403.

Robool, M.J. 1973. Historic volcanic activity at Deception Island. British Antarctic Survey Bulletin 32: 23-30.

Robool, M.J. 1979. A model for the eruptive mechanism of Deception Island from 1820 to 1970. British Antarctic Survey Bulletin 49: 137-156.

Self, S.; Sparks, R.S.J. 1981. Tephra Studies: 481 p. Springer, New York.

Shultz, C.H. 1972. Eruption at Deception Island, Antarctica, August 1970. Geological Society of America Bulletin 83: 2837-2842.

Smellie, J.L. 1990. Graham Land and South Shetland Islands. *In* Volcanoes of the Antarctic Plate and Southern Oceans (LeMasurier, W.E.; Thomson, J.W.; editors). AGU Antarctic Research Series 48: 302-353.

Smellie, J.L. 1999a. The upper Cenozoic tephra record in the South Polar region: a review. Global and Planetary Change 21: 51-70.

Smellie, J.L. 1999b. Lithostratigraphy of Miocene-Recent, alkaline volcanic fields in the Antarctic Peninsula and eastern Ellsworth Land. Antarctic Science 11 (3): 362-378.

Smellie, J.L. 2001. Lithostratigraphy and volcanic evolution of Deception Island, South Shetland Islands. Antarctic Science 13 (2): 188-209.

Smellie, J.L. 2002. The 1969 subglacial eruption on Deception Island (Antarctica): events and processes during an eruption beneath a thin glacier and implications for volcanic hazards. *In* Volcano-ice interactions on Earth and Mars (Smellie, J.L.; Chapman, M.G.; editors). Geological Society of London, Special Publications 202: 59-79.

Smellie, J.L.; Hole, M.J. 1997. Products and processes in Pliocene-Recent, subaqueous to emergent volcanism in the Antarctic Peninsula: examples of englacial Surtseyan volcano construction. Bulletin of Volcanology 58 (8): 628-646.

Smellie, J.L.; Pankhurst, R.J.; Thomson, M.R.A.; Davies, R.E.S. 1984. The geology of the South Shetland Islands: VI. Stratigraphy, geochemistry and evolution. British Antarctic Survey Scientific Reports 87: 85 p.

Smellie, J.L.; Hofstetter, A.; Troll, G. 1992. Fluorine and boron geochemistry of an ensialic marginal basin volcano: Deception Island, Bransfield Strait, Antarctica. Journal of Volcanology and Geothermal Research 49: 255-267.

Smellie, J.L.; Liesa, M.; Muñoz, J.A.; Sábat, S.; Pallás, R.; Willan, R.C.R. 1995. Lithostratigraphy of volcanic and sedimentary sequences in central Livingston Island, South Shetland Islands. Antarctic Science 7: 99-114.

Smellie, J.L.; Pallás, R.; Sábat, F.; Zheng, X. 1996. Age and correlation of volcanism in central Livingston Island, South Shetland Islands: K-Ar and geochemical constrains. Journal of South American Earth Sciences 9 (3-4): 265-272.

Smellie, J.L.; López-Martínez, J.; Headland, R.K.; Hernández Cifuentes, F.; Maestro, A.; Millar, I.L.; Rey, J.; Serrano, E.; Somoza, L.; Thomson, J.W. 2002. Geology and geomorphology of Deception Island. BAS GEOMAP Series, Sheets 6-A and 6-B. British Antarctic Survey, Cambridge: 78 p.

Smellie, J.L.; Nelson, A.; Williams, M. 2006a. Fire and ice: unraveling the climatic and volcanic history of James Ross Island, Antarctic Peninsula. Geology Today 22 (6): 220-226.

Smellie, J.L.; McIntosh, W.C.; Esser, R.; Fretwell, P. 2006b. The Cape Purvis volcano, Dundee Island (northern Antarctic Peninsula): late Pleistocene age, eruptive processes and implications for a glacial palaeoenvironment. Antarctic Science 18 (3): 399-408.

Smellie, J.L.; Johnson, J.S.; McIntosh, W.C.; Esser, R.; Gudmundsson, M.T.; Hambrey, M.J.; van Wyk de Vries, B. 2008. Six million years of glacial history recorded in volcanic lithofacies of the James Ross Island Volcanic Group, Antarctic Peninsula. Palaeogeography, Palaeoclimatology, Palaeoecology 260 (1-2): 122-148.

Smellie, J.L.; Rocchi, S.; Armienti, P. 2011. Late Miocene volcanic sequences in northern Victoria Land, Antarctica: products of glaciovolcanic eruptions under different thermal regimes. Bulletin of Volcanology 73 (1): 1-25.

Somoza, L.; Martínez-Frías, J.; Smellie, J.L.; Rey, J.; Maestro, A. 2004. Evidence for hydrothermal venting and sediment volcanism discharged after recent short-lived volcanic eruptions at Deception Island, Bransfield Strait, Antarctica. Marine Geology 203: 119-140.

Stenni, D.; Proposito, M.; Gragnani, R.; Flora, O.; Jouzel, J.; Falourd, S.; Frezzotti, M. 2002. Eight centuries of volcanic signal and climate change at Talos Dome (East Antarctica). Journal of Geophysical Research 107 (D9): 4076. doi: 10.1029/2000JD000317.

Stern, C. 1990. Tephrochronology of southernmost Patagonia. National Geographic Research 6 (1): 110-126.

Stern, C. 2008. Holocene tephrochronology record of large explosive eruptions in the southernmost Patagonian Andes. Bulletin of Volcanology 70 (4): 435-454.

Stothers, R.; Rampino, M. 1983. Historic volcanism, European dry fogs, and Greenland acid precipitation, 1500 B.C. to A.D. 1500. Science 222 (4622): 411-413.

Strelin, J.; Malagnino, E.C. 1992. Geomorfología de la isla James Ross. *In* Geología de la isla James Ross (Rinaldi, C.A.; editor): 7-36. Buenos Aires.

Tarney, S.D.; Saunders, A.D.; Pankhurst, R.J.; Barker, P.F. 1982. Volcanic evolution of the northern Antarctic Peninsula and Scotia arc. *In* Andesites (Thorpe, R.S.; editor). Norwich, John Wiley & Sons: 371-400.

Tatur, A.; del Valle, R.A.; Pazdur, M. 1991. Lake sediments in maritime Antarctic zone: a record of landscape and biota evolution: preliminary report. Internationale Vereinigung für Theoretische und Angewandte Limnologie 24: 3022-3024.

Timmreck, C.; Graf, H.-F. 2006. The initial dispersal and radiative forcing of a northern hemisphere mid-latitude super volcano: a model study. Atmosphere, Chemistry, Physics 6: 35-49. doi: 10.5194/acp-6-35-2006.

Traufetter, F.; Oerter, H.; Fischer, H.; Weller, R.; Miller, H. 2004. Spatio-temporal variability in volcanic sulphate deposition over the past 2 kyr in snow pits and firn cores from Amundsenisen, Antarctica. Journal of Glaciology 50 (168): 137-146.

Turner, S.P.; Hawkesworth, C.J. 1997. Constraints on flux rates and mantle dynamics beneath island arcs from Tonga-Kermadec lava geochemistry. Nature 389: 568- 573.

Turner, S.P.; George, R.M.M.; Evans, P.J.; Hawkesworth, C.J.; Zellmer, G.F. 2000. Time-scales of magma formation, ascent and storage beneath subduction-zone volcanoes. Philosophical Transactions of the Royal Society of London, A, 358: 1443-1464.

Turney, C.S.M.; Lowe, J.J.; Davies, S.M.; Hall, V.; Lowe, D.J.; Wastegård, S.; Hoek, W.Z.; Alloway, B. 2004. Tephrochronology of last termination sequences in Europe: a protocol for improved analytical precision and robust correlation procedures (a joint SCOTAV-INTIMATE proposal). Journal of Quaternary Science 19 (2): 111-120.

Valenzuela, E.; Chávez, L.; Munizaga, F. 1970. Actividad volcánica en Isla Decepción, Antártica, 1967. Serie Científica Instituto Antártico Chileno 1 (1): 25-40.

Veit, A. 2002. Vulkanologie und Geochemie pliozäner bis rezenter Vulkanite beiderseits der Bransfield-Straße / West-Antarktis. Dissertation, Alfred-Wegener-Institute, Reports on Polar and Marine Research 420: 177 p. Bremerhaven.

Walter, H.J.; Hegner, E.; Diekmann, B.; Kuhn, G.; Rutgers van der Loeff, M.M. 2000. Provenance and transport of terrigeneous sediment in the South Atlantic Ocean and their relations to glacial and interglacial cycles: Nd and Sr isotopic evidence. Geochimica et Cosmochimica Acta 64 (22): 3813-3827.

Weaver, S.D.; Saunders, A.D.; Pankhurst, R.J.; Tarney, J. 1979. A geochemical study of magmatism associated with the initial stages of back-arc spreading. The Quaternary volcanics of Bransfield Strait, from South Shetland Islands. Contributions to Mineralogy and Petrology 68: 151-169.

Wilch, T.I.; McIntosh, W.C.; Dunbar, N.W. 1999. Late Quaternary volcanic activity in Marie Byrd Land: Potential $^{40}Ar/^{39}Ar$-dated time horizons in West Antarctic ice and marine cores. GSA Bulletin 111 (10): 1563-1580.

Winchester, J.A.; Floyd, P.A. 1977. Geochemical discrimination of different magma series and their differentiation products using immobile elements. Chemical Geology 20: 325-343.

Zandomeneghi, D.; Barclay, A.; Almendros, J.; Ibáñez, J.M.; Ben-Zvi, T.; Wilcock, W.S.D.; the TOMODEC Working Group 2007. Three-dimensional P wave tomography of Deception Island Volcano, South Shetland Islands. *In* Antarctica: A Keystone in a Changing World - Online Proceedings of the 10th ISAES (Cooper, A.K.; Raymond, C.K.; editors), USGS Open-File Report 2007-1047, Extended Abstract 025: 4 p.

Zandomeneghi, D.; Barclay, A.; Almendros, J.; Ibáñez Godoy, J.M.; Wilcock, W.S.D.; Ben-Zvi, T. 2009. Crustal structure of Deception Island volcano from P wave seismic tomography: Tectonic and volcanic implications. Journal of Geophysical Research 114, B06310. doi: 10.1029/2008JB006119.

Zielinski, G.A.; Dibb, J.E.; Yang, Q.; Mayewski, P.A.; Whitlow, S.; Twickler, M.S.; Germani, M.S. 1997. Assessment of the record of the 1982 El Chichón eruption as preserved in Greenland snow. Journal of Geophysical Research 102 (D25): 30031-30045. doi: 10.1029/97JD01574.

Manuscript received: October 03, 2011; revised/accepted: April 13, 2012; available online: July 25, 2012.